

Hygroscopicity of organic surrogate compounds from biomass burning and their effect on the efflorescence of ammonium sulfate in mixed aerosol particles

Ting Lei^{1,2}, Andreas Zuend⁴, Yafang Cheng^{2,3}, Hang Su^{2,3}, Weigang Wang¹, Maofa Ge^{1*}

¹State Key Laboratory for Structural Chemistry of Unstable and Stable Species, CAS Research/Education Center for Excellence in Molecular Sciences, Institute of Chemistry, Chinese Academy of Sciences, Beijing, 100190, P. R. China

²Multiphase Department, Max Planck Institute for Chemistry, Mainz 55128, Germany

³Institute for Environmental and Climate Research, Jinan University, Guangzhou, China

⁴Department of Atmospheric and Oceanic Sciences, McGill University, Montreal, Quebec, Canada

Correspondence to: M. F. Ge (gemaofa@iccas.ac.cn)

Abstract: Hygroscopic growth factors of organic surrogate compounds representing biomass burning and mixed organic-inorganic aerosol particles exhibit variability during dehydration experiments depending on their chemical composition, which we observed using a hygroscopicity tandem differential mobility analyzer (HTDMA). We observed that levoglucosan and humic acid aerosol particles release water upon dehumidification in the range from 90 – 5 % relative humidity (RH). 4-Hydroxybenzoic acid aerosol particles, however, remain in the solid state both upon dehumidification or dehumidification and exhibit a small shrinking in size at higher RH compared to the dry size. For example, the measured growth factor of 4-hydroxybenzoic acid aerosol particles is ~0.96 at 90 % RH. The measurements were accompanied by RH-dependent thermodynamic equilibrium calculations using the AIOMFAC and the E-AIM models, the ZSR relation, and a fitted hygroscopicity expression. We observed several effects of organic components on the hygroscopicity behavior of mixtures containing ammonium sulfate (AS) in relation to the different mass fractions of organic compounds: (1) a shift of efflorescence relative humidity (ERH) of ammonium sulfate to higher RH due to the presence of 25 wt % levoglucosan in the mixture. (2) There is a distinct efflorescence transition at 25 % RH for mixtures consisting of 25 wt % of 4-hydroxybenzoic acid compared to the ERH at 35 % for organic-free AS particles. (3) There is indication for a liquid-to-solid phase transition of 4-hydroxybenzoic acid in the mixed particles during dehydration.

(4) A humic acid component shows no significant effect on the efflorescence of AS in mixed aerosol particles. In addition, consideration of a composition-dependent degree of dissolution of crystallization AS (solid-liquid equilibrium) in the AIOMFAC and E-AIM models leads to a relatively good agreement between models and observed growth factors, as well as ERH of AS in the mixed system. The use of the ZSR relation leads to good agreement with measured diameter growth factors of aerosol particles containing humic acid and ammonium sulfate. Lastly, two distinct mixtures of organic surrogate compounds, including levoglucosan, 4-hydroxybenzoic acid, and humic acid were used to represent the average water-soluble organic carbon (WSOC) fractions observed during the wet and dry seasons in the central Amazon Basin. A comparison of the organic fraction's hygroscopicity parameter for the simple mixtures, e.g. $\kappa \approx 0.12$ to 0.15 for the wet-season mixture in the 90 % to 40 % RH range, shows good agreement with field data for the wet season in Amazon (WSOC $\kappa \approx 0.14 \pm 0.06$ at 90 % RH). This suggests that laboratory-generated mixtures containing organic surrogate compounds and ammonium sulfate can be used to mimic, in a simplified manner, the chemical composition of ambient aerosols from the Amazon for the purpose of RH-dependent hygroscopicity studies.

Introduction

It is well established that biomass burning, as an important source of atmospheric aerosol particles, has a wide range of climate effects that can be classified into direct radiative effects through light-absorbing carbon aerosol particles and indirect effects by impact on cloud condensation nuclei and cloud microphysics (Andreae and Gelencsér, 2006; Moosmüller et al., 2009; Hecobian et al., 2010; Rizzo et al., 2011; Rose et al., 2011; Cheng et al., 2012; Engelhart et al., 2012; Lack et al., 2012; Jacobson, 2014; Liu et al., 2014; Saleh et al., 2013, 2014). Atmospheric light-absorbing particles that arise from biomass burning play an important role as a driver of global warming (Favez et al., 2009; Hegg et al., 2010; Lack et al., 2012; Feng et al., 2013; Laborde et al., 2013; Srinivas and Sarin, 2013). According to the IPCC report (Boucher and David, 2013), the climate forcing of black carbon aerosol particles may rival that of methane, with a present-day global warming effect of up to $0.3\text{--}0.4\text{ }^{\circ}\text{C}$ (Wang et al., 2014). Also, certain types of aerosol particles emitted by biomass burning, when immersed into cloud droplets, absorb solar radiation and facilitate water evaporation and cloud dispersion, which indicates an additional indirect aerosol effect that counteracts the cooling effect of cloud droplets nucleated by aerosols (Powelson et al., 2014). Therefore, a better understanding of the influence of aerosol particles from biomass burning on

cloud formation, precipitation, and Earth's radiative budget is required to comprehend biomass burning aerosol properties and behavior.

The understanding of aerosol-cloud-climate impact of a vast range of biomass burning derived organic compounds, however, is rather limited due to the complexity of biomass burning emissions, gas- and aerosol-phase processing and the restricted availability of field measurements (Pratt et al., 2011; Lei et al., 2014; Paglione et al., 2014; Srinivas and Sarin, 2014; Zhong and Jang, 2014; Ciarelli et al., 2015; Arnold et al., 2015; Lawson et al., 2015; Gilman et al., 2015). Moreover, biomass burning particles are often mixtures of water-soluble organic carbon, black carbon, varying amounts of inorganic components, and water insoluble inclusions, such as mineral dust or poorly soluble organics (Väkevä et al., 2002; Sadezky et al., 2005; Saarnio et al., 2010). An appreciable amount of organic compounds affect the physicochemical properties of aerosols, such as hygroscopicity, liquid-solid and liquid-liquid phase transitions, and chemical reactivity in liquid phases and/or on particle surfaces (Shiraiwa et al., 2013). For example, equilibrium between the variable environmental water vapor mixing ratio and aerosol particles may lead to substantial changes in particle size, and chemical composition, all of which can influence light absorption and scattering (Seinfeld and Pandis, 2006; Zhang et al., 2016). RH-dependent transitions between solid and liquid (aqueous) phases are also important in determining optical properties (Martin et al., 2013; Wang et al., 2010; Kim et al., 2016; Wu et al., Denjean et al., 2015; 2016; Hodas et al., 2015; Atkinson et al., 2015). Studies have shown that water-soluble organic matter from biomass burning (approximately 70 % of total organic matter) can significantly suppress, enhance or have no effect on the deliquescence (e.g. the RH at which deliquescence occurs at a certain temperature, the DRH) and efflorescence process (e.g. the efflorescence RH, ERH) of present inorganic electrolytes. The effect depends predominantly on the type of organics, mass fraction of organics relative to inorganic, and particle size (You and Bertram, 2014; Zawadowicz et al., 2015; Hodas et al., 2015; Gupta et al., 2015). Whole particles, individual phases within particles, or specific chemical compounds can undergo a range of phase transitions including crystallization/efflorescence, dissolution/deliquescence, and liquid-liquid phase separation as the relative humidity varies in the atmosphere. A number of laboratory studies have focused on liquid-liquid phase separations within particles consisting of inorganic and organics fractions (Svenningsson et al., 2006; Carrico et al., 2008; Dusek et al., 2011; Hodas et al., 2015). For example, studies about liquid-liquid separation occurring in mixed organic-inorganic aerosols were performed by

Song et al. (2012, 2013) and You et al. (2013) using Raman and optical microscopy, establishing that liquid-liquid phase separation occurs typically in mixed organics + ammonium sulfate particles with an average elemental oxygen-to-carbon (O:C) ratio of the organic fraction of less than 0.6 and in some cases for $0.6 < \text{O:C} < 0.8$. You et al. (2013) further found that for a O:C ratio between 0.5 and 0.8, the occurrence of liquid-liquid phase separation at moderate to high RH depends on the types of inorganic salts present (i.e., the effective strength of the salting-out effect), e.g., $(\text{NH}_4)_2\text{SO}_4 \geq \text{NH}_4\text{HSO}_4 \geq \text{NaCl} \geq \text{NH}_4\text{NO}_3$. Recently, the effect of a potential size-dependent morphology and dependence of the phase separation mechanism on the organic/inorganic mass ratio in mixed aerosol was studied for mixtures of poly- (ethylene glycol)-400 + ammonium sulfate using cryogenic-transmission electron microscopy (Altaf et al., 2016). Therefore, many independent studies suggest that the occurrence of solid-liquid and/or liquid-liquid phase separations, as well as related (temperature-dependent) RH levels of phase transitions (DRH, ERH, SRH), depend on the relative amounts of organic and inorganic aerosols components and their non-ideal mixing behavior.

The expected physical state and morphology of aerosol particles containing mixtures of a wide range of organic and inorganic salts/acids can, in principle, be predicted by a selection of specialized thermodynamic equilibrium models. Such models include the Extended Aerosol Inorganic Model (E-AIM) (Clegg and Seinfeld, 1998, 2006; available online: <http://www.aim.env.uea.ac.uk/aim/aim.php>), the Aerosol Diameter Dependent Equilibrium Model (ADDEM) (Topping et al., 2004), the UNiVersal Quasichemical Functional Group Activity Coefficients model (UNIFAC) (Fredenslund et al., 1975; Hansen et al., 1991), and the Aerosol Inorganic-Organic Mixtures Functional groups Activity Coefficients model (AIOMFAC) (Zuend et al., 2008, 2011, 2012). These models have all been used to predict atmospheric aerosol thermodynamic equilibrium for a variety of inorganic and organic systems, yet not all of them can be used to compute non-ideal mixing in organic-inorganic systems. AIOMFAC has been used to predict the distribution of components in multiple phases in a range of mixed organic-inorganic systems and demonstrated its broad applicability in predicting liquid-liquid phase separation in such mixtures (Zuend et al., 2010; Song et al., 2012; Zuend and Seinfeld, 2012; Shiraiwa et al., 2013; Renbaum-Woff et al., 2016; Rastak et al., 2017).

Several previous experimental studies using the HTDMA technique (e.g. Zardini et al., 2008; Lei et al., 2014) show that the deliquescence of inorganic compounds is affected by the presence of organic

components, which manifests itself in a shift in the DRH of a salt compared to the corresponding organic-free system. For instance, a clear shift of ammonium sulfate DRH was observed in the case of the levoglucosan + ammonium sulfate system (Lei et al., 2014). Here we focus on investigating the morphology, hygroscopicity and phase transitions of relevant organic compounds found in biomass burning aerosol during the dehydration/dehumidification process. Moreover, we study how the presence of organic compounds affects the water loss behavior of mixed organic-inorganic aerosols with ammonium sulfate (AS) in the supersaturated state as well as after efflorescence of AS. In addition, we compare the measured hygroscopicity behavior of mixed aerosol particles with predictions from the Zdanovskii–Stokes–Robinson (ZSR) mixing rule, the E-AIM model and the AIOMFAC model.

2 Methods

2.1 Aerosol system

The three organic compounds levoglucosan, 4-hydroxybenzoic acid and humic acid were used as surrogates for the rich-class of water-soluble organic components in biomass burning aerosols. The influence of the distinct chemical structure of these compounds was studied with regard to the water uptake and evaporation of the pure organic compounds as well as for mixed organic-AS-containing particles. Furthermore, a comparison with field data from the Amazon was performed to quantify the ability of mixtures of these three organic compounds to mimicking the hygroscopic behavior of complex ambient organic particles originating from biomass burning emissions. Here we focus on the characterization of hygroscopic growth factors as well as solid-liquid and liquid-liquid phase transitions during the dehumidification conditions. The chemical substances and their physical properties are characterized in Table 1. All of the experimental solutions were prepared by dissolving in Milli-Q water (resistivity $\geq 18.2 \text{ M}\Omega$) and the experiments were conducted at room temperature ($\sim 298 \text{ K}$). For the mixtures of ammonium sulfate and organic surrogates the different mass ratios of AS: organic considered are 3:1, 1:1 1:3. The chemical compositions of biomass-burning model mixtures are introduced in Table 2.

2.2 Instrument design

Figure 1 shows a schematic of the HTDMA instrument, more detailed information about this instrument's setup, calibration and evaluation is described elsewhere (Lei et al., 2014; Jing et al., 2015, 2017; Liu et al., 2015). Briefly, Poly-dispersed sub-micrometer aerosol particles are generated by atomizing (MSP 1500, MSP) a 0.05 weight % aqueous solution consisting of different mass fractions of inorganic, and organic components, assuming that the composition of the formed aerosol particles is initially the same as that of the solution used in the atomizer. Aerosol particles from an atomizer are routed through homemade silica diffusion dryers and then pass through a Nafion gas dryer (Perma Pure Inc., USA). After aerosol particles were dried to below 5 % RH (RH set point 1, RH1), they are directed to the impactor; those aerosols with diameter less than 1 μm are allowed to pass it and subsequently pass through a ^{85}Kr electric charger to reach a near-Boltzmann distribution of charges (Liu et al., 1985). After charging, the aerosol particles enter the first differential mobility analyzer (DMA1) at a sheath flow to aerosol flow ratio of 4:0.3. The sheath flow is circulated by the diaphragm pump in the first loop DMA1 system, and its RH is kept constant at below 5 % RH. The resulting mono-disperse particle population, selected within uncertainty by the DMA1, is then exposed to high RH conditions during which the aerosol flow is humidified to 98 % RH by mixing water through a Nafion membrane humidifier at 30 °C. After passing through a saturator (Perma Pure Inc., USA), the aerosols are dried to a target RH level (RH2) through a series of two single-Nafion tubes (Perma Pure Inc., USA) with RH2 set to a value in the range of 90 % to 5 % RH. Here, a pulse width modulator (PWM) circuit is used to regulate the sheath flow on the basis of a proportional integral derivative (PID) system. When the second Nafion membranes allow for regulating the sheath flow to a desired RH and for controlled flow into the sample stream until the RH2 setting value is equal to the excess RH of sheath flow value (RH3), the mobility diameter of the dehumidified aerosols at target RH are measured with the second DMA (DMA2, a scanning DMA) coupled with a condensation particle counter CPC (Model 1500, MSP). In addition, the residence time between the humidifier and DMA2 is around 5 s, which is estimated to be sufficient for aerosols to grow/shrink to equilibrium size at a certain RH setpoint. Also, due to recirculation of the sheath flow and the pre-humidification of the aerosol flow, the sheath flow and aerosol sample flow are enabled to rapidly reach the same RH.

2.3 Theory and modeling methods

Models were applied to explore the extent to which measured hygroscopic diameter growth factors

(HGFs), particle phase states, and phase compositions under sub-saturation conditions can be predicted by thermodynamic equilibrium models. For the AS-containing systems studies, the current thermodynamic equilibrium predictions account for a crystalline AS phase with solid-liquid equilibria prior to the complete deliquescence of AS under hydration conditions. Similarly, the crystallization point followed by a solid-liquid equilibrium of AS needs to be considered to predict the effect of organic components in the mixed particles on the shift/suppression of AS efflorescence during aerosol dehumidification, i.e. referring to processes occurring along the dehydration branch of a HTDMA humidification-dehumidification cycle. The calculation of the ERH of AS in an organic-inorganic solution is thermodynamically related to the solubility limit, but it is not strictly deterministic (unlike the DRH) due to the stochastic nature of nucleation-and-growth of a crystal embryo. The molality of pure AS at saturation in an aqueous solution is known, e.g. measured by Apelblat (1993) at 298.15 K as $m_{AS}^{(sat)} = 5.790$ mol/kg, while measurements are most often not available for the solubility limit of AS in aqueous inorganic-organic systems. However, crystalline AS in equilibrium with an aqueous mixture demonstrates a specific molal ion activity product (IAP) in that solution at a given temperature and atmospheric pressure. For example, in the case of a ternary liquid mixture of levoglucosan + AS + water in solid-liquid equilibrium (SLE) with a crystalline AS phase at a certain temperature T, a constant molal ion activity product $IAP_{AS} = IAP_{AS}^{(sat)}(T)$ is established (necessary SLE condition). In this case the liquid mixture is a so-called saturated solution with respect to AS. While the molar amount of AS in a saturated solution depends on the other mixture constituents, the value of $IAP_{AS}^{(sat)}(T)$ is a function of temperature only, since it is derived from the fixed chemical composition and associated chemical potential of the crystalline phase. A reference value for $IAP_{AS}^{(sat)}(T)$ can therefore be calculated with the AIOMFAC model from an experimentally determined solubility limit of AS in a known mixtures, such as the molality of AS at the point of saturation in the binary aqueous system (water + AS). The RH at which full dissolution of a solid phase upon humidification is just reached, the DRH, is directly related to the conditions at which a saturated solution becomes subsaturated upon addition of water. Here the degree of saturation with AS can be determined unambiguously by the computed value of IAP_{AS} as a function of mixture composition and temperature. Making use of these thermodynamic relationships, the AIOMFAC-based equilibrium model is used to calculate the DRH and ERH of AS in the multicomponent system, as outlined below. Detailed information on the modeling of solid-liquid equilibria and the IAP-based prediction of ERH is given in Zuend et al. (2011) and Hodas et al. (2016). Briefly, the ERH is

determined based on the following equations:

$$IAP_{AS} = \left[a_{NH_4^+}^{(m)} \right]^2 \left[a_{SO_4^{2-}}^{(m)} \right]^1 \quad (1)$$

$$IAP_{AS}^{[crit]} = c_{AS} \times IAP_{AS}^{(sat)} \quad (2)$$

Here $a_{NH_4^+}^{(m)}$ and $a_{SO_4^{2-}}^{(m)}$ are the molal activities of the ammonium and sulfate ions in solution (Zuend et al., 2010). Molality basis is indicated by superscript “(m)” (which is not a mathematical exponent). $IAP_{AS}^{(sat)}$ denotes the molal ion activity product of AS at salt saturation computed by the thermodynamic equilibrium model for any aqueous AS system at a certain temperature (here 298.15 K). The calculated molal IAP at saturation of the corresponding binary salt solution is taken as the (known) reference value. The RH at which this $IAP_{AS}^{[sat]}$ value is just reached in certain bulk solution at equilibrium with its environment (in contrast to $IAP_{AS} < IAP_{AS}^{(sat)}$ at higher RH), is the (bulk) DRH of AS. Similarly, the ERH is determined at the point of crystallization by a critical IAP value denoted as $IAP_{AS}^{[crit]}$ (Hodas et al., 2016), the value of $IAP_{AS}^{[crit]} > IAP_{AS}^{[sat]}$ expresses the need for reaching a critical IAP threshold (critical level of AS super-saturation) for highly likely nucleation-and-growth of a new crystalline AS phase. The multiplication factor c_{AS} is used as a constant coefficient relating the IAP at AS saturation to the one expected at the point of crystallization in aqueous mixed particles. From the comparison of laboratory measurement of ERH for aqueous AS solution to the AIOMFAC-predicted IAP_{AS} at that RH, the value of $c_{AS} \approx 30$ was determined; this value is in particular applicable to submicron-sized AS droplets (Zardini et al., 2008; Ciobannu et al., 2010).

An analogous approach is used for the ERH predictions with the E-AIM model, however, since E-AIM provides activity coefficients and activities on mole fraction basis, denoted here by superscript “(x)” (rather than molality basis), the value of $c_{AS}^{(x)}$ need to be determined separately for that model. Expressing Eq. (1) by mole-fraction-based activities of NH_4^+ and SO_4^{2-} and comparison to the $IAP_{AS}^{(sat,x)}$ and $IAP_{AS}^{(crit,x)}$ computed by E-AIM for AS at the experimental solubility limit and ERH in aqueous AS solutions, a value of $c_{AS}^{(x)} \approx 40$ was determined for the calculation with E-AIM.

As discussed by Lei et al. (2014), predicting of hygroscopic growth factors with E-AIM includes a sophisticated composition-dependent solution density model, which considers the non-ideality effects on apparent molar volumes used for the calculation of the solution density in mixed organic-inorganic

systems (Clegg and Wexler, 2011a, b). The AIOMFAC-based model applies a simpler solution density treatment by assuming that the partial molar volumes of solution species are independent of non-ideal interactions, i.e. the mixed solution density is calculated based on linear additivity of pure component solid or liquid volume contributions to obtain the HGF at a given RH. Differences in the density models are expected to lead to relatively small differences, typically on the order of the HTDMA measurement error or less (e.g. Fig. 2a), in the application to HGF predictions, as demonstrated by Lei et al. (2014) for the case of diameter vs. mass-based HGF of AS droplets. Both models include sophisticated sets of equations to compute activity coefficients of all solution components in a thermodynamically consistent manner.

2.4 κ -Köhler theory and computation of the hygroscopicity parameter κ

The hygroscopicity parameter, κ , is commonly used to characterize the relative hygroscopicities of individual aerosol particles, known mixtures or complicated atmospheric aerosols (Petters and Kreidenweis, 2007), and to model the composition-dependence of the solution water activity. The saturation ratio, S , in the traditional Köhler equation (Eq. 3), over an aqueous droplet is calculated from

$$S = a_w \left(\frac{4\sigma_s M_w}{RT \rho_w D_{wet}} \right) \quad (3)$$

Where a_w is the mole-fraction-based water activity in solution, M_w and ρ_w are the molar mass of water and the density of pure water in the liquid state at temperature T , respectively. D_{wet} , the “wet” particle diameter at a given RH, is defined by $D_{wet} = HGF \times D_0$. D_0 denotes the diameter at dry conditions at RH below 5 %. The solution surface tension is denoted by σ_s . In the “ κ -Köhler theory”, the bulk solution water activity is described by a single parameter κ , with the hygroscopic parameter of the overall mixture related to Eq. (3) by

$$\kappa_{HGF} = 1 - HGF^3 + \frac{HGF^3 - 1}{S} \exp \left[\frac{4\sigma M_w}{RT \rho_w D_{wet}} \right] \quad (4)$$

This expression describes effective values of κ_{HGF} as a function of droplet diameter and HGF at a certain saturation ratio. In turn, known (measured) solution κ_{HGF} values or component-specific κ_i values can be used to parameterize or predict the HGF curve of a mixture (Petters and Kreidenweis, 2007).

2.5 GF data fit

As described by Dick et al. (2001), the relationship between measured hygroscopic growth factors and water activity can alternatively be parameterized by the following expression:

$$HGF = \left[1 + (c_1 + c_2 \times a_w + c_3 \times a_w^2) \frac{a_w}{1-a_w} \right]^{\frac{1}{3}} \quad (5)$$

By substitution of Eq. (3) for a_w in Eq. (5) and a fit to the measured HGF the three adjustable coefficients c_1 , c_2 , c_3 of Eq. (5) were determined. The coefficient values are given in Table 3 for the different organic compounds considered.

2.6 GF prediction by ZSR

The Zdanovskii-Stokes-Robinson mixing rule is widely used to approximate the water uptake of mixed systems by assuming additivity of the water uptake of each individual component in the mixed particles at a given RH (e.g., Malm and Kreidenweis, 1997). HGF_{mix} is based on the HGF_j of pure components j and their corresponding volume fraction, ε_j in the mixed particles.

$$HGF_{mix} = \left[\sum_j \varepsilon_j (HGF_j)^3 \right]^{\frac{1}{3}} \quad (6)$$

3. Results and discussion

3.1 GF of single compounds systems

Figure 2a shows the measured diameter growth factors of AS particles as a function of RH for both humidification and dehumidification conditions. The measured ERH of 100 nm AS particles is approximately 35 % RH at 298.15 K. The models predicted GF and predicted solid-liquid phase transition of AS are in relatively good agreement with the experimental data and, in particular, the efflorescence (crystallization) of AS is captured by the AIOMFAC and E-AIM models. The good model-measurement agreement for the ERH is of course expected, since the aqueous AS system serves as the reference system for determining the value pairs of $IAP_{AS}^{(sat)}$ and c_{AS} on molality and mole fraction basis for use with AIOMFAC and E-AIM, respectively (section 2.3). An ERH of 31 % to 40 % RH was reported by other groups for a range of particle sizes and experimental techniques (Zardini et al., 2008; Ciobanu et al.,

2010). There are several factors that contributed to the variability of reported ERH values, such as particles size, temperature, solution impurities and the stochastic nature of the homogeneous or heterogeneous nucleation of a crystalline phase near ERH (Ciobanu et al., 2010).

In Fig. 2b, upon dehydration, no efflorescence of the levoglucosan aerosol particles is observed even at RH below 10 %. The agreement of the HGF between the hydration and dehydration processes demonstrates that these particles equilibrate with the surrounding water vapor under these moisture conditions. For example, the measured diameter growth factors of levoglucosan particles at 80, 60, and 30 % RH are 1.19, 1.09, and 1.03, respectively, which are similar to results obtained for the hydration process of such particles. Levoglucosan has a DRH of ~80 % to 83 % (for a bulk system) at 293 to 298 K (Mochida and Kawamura, 2004; Zamora et al., 2011). The similarity of diameter growth factors both under hydration and dehydration conditions even below the DRH of levoglucosan is explained by the lack of crystallization of levoglucosan upon drying to low RH and the presence of a metastable supersaturated aqueous levoglucosan solution in both the hydration and dehydration modes for experiments initiated with liquid solution droplets (Mochida and Kawamura, 2004; Chan et al., 2005; Svenningsson et al., 2006). A possible reason for a persistent metastable supersaturated solution states is that levoglucosan particles remain liquid (possibly a viscous liquid state) upon drying to below 5 % RH, which was also observed previously with a reported ERH < 4% RH (Mochida and Kawamura, 2004; Chan et al., 2005). Also, the measured diameter growth factors of levoglucosan particles are in good agreement with these estimated from the standard UNIFAC model within the E-AIM model and the AIOMFAC model, within experimental uncertainty. The UNIFAC models within E-AIM and AIOMFAC are based on the original model expressions by Fredenslund et al. (1975) and both include the extensive parameter set by Hansen et al. (1991) as well as revised parameters for certain group interactions of water with carboxyl and hydroxyl groups by Peng et al. (2001). Of relevance for levoglucosan and other sugar-like compounds, the AIOMFAC model also contains certain revised group parameters for hydroxyl groups and special alkyl groups for their interactions with water, introduced by Marcolli and Peter (2005) for polyols, as further detailed in Zuend et al. (2011). However, the molecular structure of levoglucosan with several polar functional groups in close vicinity may account for a small deviation between models and measured *HGFs* at RH below 70 %, because intramolecular interactions are not fully considered by these models.

The measured diameter growth factors of 4-hydroxybenzoic acid particles shown in Fig. 2c demonstrate untypical increase in diameter of 4-hydroxybenzoic acid particles during dehumidification from 90 to 10 % RH, which is consistent with previous diameter growth factor for a few solid particles (Mochida and Kawamura, 2004). The organic particles measured are likely always in the effloresced, i.e. crystalline state apparently even at high RH. The apparent increase in diameter during dehumidification may be explained by particle shape restructuring, since the (poly)-crystalline particles are likely non-spherical at dry conditions, but may become more sphere-like in shape when exposed to higher RH (Mikhailov et al., 2004). Also, no ERH of 4-hydroxybenzoic acid in the dehydration mode was observed during the experiments; the likely reason is that the highest RH reached in the humidifier was approximately 98 %, which may be below the ERH of 4-hydroxybenzoic acid, reported as above 98 % RH in another study (Mochida and Kawamura, 2004). As discussed previously by Lei et al. (2014), our HTDMA experiments are carried out such that RH = 98 % is reached initially before dehumidification to a series of relative humidities at set point RH2 (90 % – 5 % RH), the crystallization of the organic, however, could occur at above 90 % RH. In addition, deviations between measurements and model prediction are obvious in Fig. 2c. The observations surpass by far the expected error in model performance, which is typically less than 0.05 in HGF units for RH < 85 %, as indicated also by an intercomparison of the AIOMFAC and E-AIM predictions in Fig. 2c and much improved model-measurement agreement for the case of mixed 4-hydroxybenzoic acid + AS particles shown in Fig. 4 (discussed in Section 3. 2. 2). However, note that the validity of the shown model predictions in Fig. 2c depends on whether the assumption of a liquid solution droplet is plausible. Therefore, it is no surprise that the model-predicted curves deviate from the experimental hygroscopic behavior of 4-hydroxybenzoic acid particles. Morphology effects, such as the restructuring of non-spherical polycrystalline particles over a certain RH range or liquid-liquid phase-separated particles of non-spherical shapes, have been discussed by several groups (Sjogren et al., 2007; Reid et al., 2011; Lei et al., 2014). In the case of hygroscopic growth and deliquescence under hydration conditions for 4-hydroxybenzoic acid particles and mixtures of 4-hydroxybenzoic acid with ammonium sulfate. An offset between measurement and model predictions was observed both in the RH range below the deliquescence of the particles and above it, i.e. above 80 % RH, (Lei et al., 2014). It is suggested that deviations are primarily caused by a change in solid-state particle morphology during hydration, leading to a restructuring of the polycrystalline particle shape towards more compact, near-spherical shape as the RH

approaches the particle deliquescence point. This would explain rather uncommon HGF values of less than 1.0 at elevated RH also shown in Fig. 2c. Similar behavior was found for experimental growth factors of mixtures containing adipic acid and AS and systematic deviations between the associated ZSR predictions and observations by Sjogren et al. (2007). Thus, while experimental data hint to the possible influence of non-spherical particles and their humidity-induced restructuring as a source of uncertainty, model predictions of HGF, such as those with the AIOMFAC model, assume by default a spherical particle shape even for solid phases and/or in cases where LLPS is present.

The measured HGF curves of humic acid aerosol particles during dehumidification and humidification measurements do not agree very well within experimental uncertainty, in particular above 70 % RH. For instance, the growth factor of humic acid aerosol particles at 80 % RH is 1.2 according to the dehumidification measurement, which is higher than hygroscopic growth factor of humic acid particles in the humidification mode at the same RH. Humic acid aerosol particles shrink continuously due to loss of water content in the range from 90 % to 10 % RH. For example, a stepwise change in the water absorption and desorption behavior within different RH range was observed in the case of Nordic Aquatic Fulvic Acid (NAFA) and Suwannee River Fulvic Acid (SRFA) by Chan and Chan (2005). These hygroscopic behaviors suggest that humic acid particles and structurally similar compounds remain some water down to the low RH levels achieved in the instruments (imperfect drying during particle residence in the instrument). In addition, the experimental growth factor of humic acid aerosol particles during dehumidification can be represented well by fitting Eq. (5) to the measurements. The determined fit parameters are listed in Table 3. The humic acid sample used (Aldrich, 99%) are a mixture of different poly-carboxylic acids of undefined chemical structure. However, specific information on the chemical structure and mixture composition is necessary for corresponding model predictions with AIOMFAC and E-AIM. Therefore, no such model calculations are shown in Fig. 2d.

3.2 GF of mixtures of organic surrogate compounds + ammonium sulfate

Biomass burning aerosol particles are likely mixtures of a diversity of inorganic constituents and organic compounds in the atmosphere. For example, particles may consist of a combination of ammonium sulfate mixed with low- and semi-volatile organics from biomass burning emissions (Lee et al., 2003; Zhang et al., 2007; Pratt and Prather, 2010). Different water solubilities, and hygroscopic behavior of distinct

organic compounds may affect the hygroscopic growth factors of mixtures of partially or fully dissolved inorganic and organic components. For example, Bodsworth et al. (2010) studied the effect of different mass fractions of citric acid on the efflorescence properties of mixed citric acid-ammonium sulfate particles at lower temperature and concluded that adding citric acid decreases the ERH of ammonium sulfate in the mixed aerosol particles. These hygroscopic behaviors of mixed aerosol particles, including phase transition in the range from moderate to low RH, are the focus of attention in this study.

3.2.1 Mixed system: levoglucosan + ammonium sulfate

Figure 3 shows measured growth factors of mixed aerosol particles containing levoglucosan + ammonium sulfate with different dry state organic-to-inorganic mass ratios (1:3, 1:1, 3:1) in the RH range from 90 % to 10 %. There is a reduction in the diameter growth factor of aerosol particles containing levoglucosan and AS with increasing levoglucosan mass fraction, as expected from a ZSR-like additivity concept of hygroscopicity. When the concentration of levoglucosan is low (25 wt %), a clear efflorescence signature of AS found, within the ERH shifting to a higher RH (40 % - 45 %) in comparison to the ERH of pure AS occurring at 33 %-35 % RH (Fig.3a). A similar phenomenon has been found for the certain mixtures of NaCl and Nordic Aquatic Fulvic Acid (NAFA), in which the crystallization of NaCl shifted to higher RH by mixing with NAFA at a mass ratio of 1:1 (Chan and Chan. 2003). With increasing mass fraction of levoglucosan (i.e., 50 wt % and 75 wt %), the mixtures release water gradually and no crystallization of AS was observed. Although a small step in the growth factor curve might have occurred (indicative of the crystallization of AS), it cannot be detected with sufficient certainty by our measurement setup. The rather high viscosity of solutions containing levoglucosan is expected to increase considerably toward RH (Marshall et al., 2016). This increase in viscosity might impede the crystallization of AS in the mixed systems on the time scale of the experiment. Mass transfer limitation effects on the deliquescence or efflorescence process of crystalline organic particles and the water uptake or evaporation have been investigated in several experimental studies (Peng et al., 2001; Choi and Chan, 2002; Chan and Chan, 2005; Sjogren et al., 2007; Zardini et al., 2008; Ciobanu et al., 2010; Smith et al., 2012; Mikhailov et al., 2013; Hodas et al., 2015). Mass transfer limitations may impact the outcome of experiments significantly if the characteristic time scales for equilibration is similar to or larger than the residence time of particles in the experimental setup. In this study, the total residence time of the aerosol sample during the equilibration phase before entering the DMA2 is about 8 s. In order to improve the

probability that the particles reach equilibrium with the target RH during this residence time, the monodisperse aerosol selected by DMA1 is first humidified to 98 % RH. The aerosol particles are then exposed to a lower target RH by a two-step process using double Nafion tubes. Kerminen (1997) estimated the necessary residence time for achievement of water equilibrium of aqueous droplets to be between 8×10^{-6} s and 0.1 s for 100 nm and 500 nm particles, respectively. Therefore, the typical residence time of a few seconds in the humidification or dehumidification section in a HTDMA measurement is assumed to be sufficient for most equilibrium hygroscopicity measurements (Brooks et al., 2004; Mikhailov et al., 2004). Moreover, our HGF results for the three pure organic components are in good agreement with respective data by Mochida and Kawamura, (2004), Brooks et al., (2004) and Chan and Chan (2005) conducted with different techniques and/or residence times. However, there are cases where water equilibration could be impeded substantially in the presence of highly viscous or glassy particles at low RH, e.g. for ternary sucrose + NaCl + water particles of $> 6 \mu\text{m}$ in diameter studied by Bones et al. (2012), who report an equilibration time scale > 1000 s for such particles. Note that, aside from viscosity, there is an important size-dependence of the particles on the equilibration time scale (e.g. Koop et al. 2011). For aqueous 100 nm particles used in HTDMA experiments at room temperature, Bones et al. (2012) indicate that the equilibration time scale for water is likely only of concern for RH < 10 % in such an instrument. We therefore conclude that the residence time of 8 s is very likely sufficient to allow for equilibrium HGF measurements in dehydration mode, at least down to 10 % RH (when starting with aqueous solution droplets).

Mass transfer effects in hygroscopicity measurements of aerosol particles during hydration conditions have been encountered previously, particularly when a solid-liquid phase transition (deliquescence) is involved (Peng et al., 2001; Chan and Chan, 2005; Sjogren et al., 2006). For example, Peng et al. (2001) observed in electrodynamic balance (EDB) experiments under conditions of very slow humidification that glutaric acid aerosol particles showed a deliquescence phase transition in the RH range from 83 to 85 % over the course of several hours. This is a much longer time span than that of ~ 40 min for the deliquescence of other super-micron sized dicarboxylic acid particles (e.g., malonic acid) in EDB experiments. This observation indicates that the solid-liquid phase transition of glutaric acid particles may likely be mass transfer limited during the hydration process. In this context, it is possible that the deliquescence of initially solid, pure 4-hydroxybenzoic acid particles at RH > 97 % is further impeded

by slow dissolution, which could have led to the absence of deliquesced particles (Fig. 2c) on experimental time scale.

In addition, the measured diameter growth factors of mixtures of levoglucosan and AS are compared to calculations of hygroscopic growth by the E-AIM and AIOMFAC models. The E-AIM prediction is in relatively good agreement with results from the HTDMA measurement but typically overestimates the water content of particles consisting of organic-AS mixtures at the RH range close to the ERH of AS.

The liquid-solid phase transition of ammonium sulfate in the mixed particles is considered in the E-AIM assumptions as described in Section 2.3. There is a more distinct shift of ERH of AS with higher mass fractions of levoglucosan. In the case of the AIOMFAC and E-AIM model predictions, it is assumed that the diameter growth factor contribution from AS is zero below the predicted ERH, i.e. there the growth factor deviation from 1.0 is solely due to the organic water uptake. The model prediction shows a slight deviation from the measurements, which may be in part due to (i) model uncertainty in the correct description of the hygroscopicity of levoglucosan, (ii) due to incomplete representation of AS + levoglucosan interactions in aqueous solutions and (iii) in part due to measurement error. Also, in the case of mixtures consisting of AS and levoglucosan with organic-to-inorganic dry mass ratio of 3:1 (75 wt % levoglucosan of dry particle composition), the underestimation of the growth factor by the AIOMFAC model at $RH < 35\%$ in comparison to the measurements is explained in part by the model prediction of AS efflorescence (which seems to be absent in the measurements). However, with decreasing AS mass fraction, the hygroscopic behavior of levoglucosan dominates the diameter growth factors of the mixtures, in relative agreement with the AIOMFAC-modeled “dehydration branch” prediction. Minor differences in the AIOMFAC prediction vs. -measurement for diameter growth factors of mixed levoglucosan and AS in the RH range of 35 - 25 % here might be attributed to mixture viscosity effects at the higher levoglucosan contents, which may suppress the efflorescence of AS in the mixed systems on experimental timescale or it could simply be due to sufficient miscibility of dissolved AS in the aqueous levoglucosan solution (beyond that predicted by the model), such that a small step-change due to AS efflorescence could be beyond the experimental detection range. As a result, accounting for the effect of the organic components on the diameter growth factors of mixtures within aerosol particles is crucial to model accurately the equilibrium hygroscopic behavior.

3.2.2 Mixed system: 4-hydroxybenzoic acid + ammonium sulfate

Mixtures of 4-hydroxybenzoic acid + AS with different organic mass fraction (25, 50, 75 wt %) exhibit a gradual water desorption before the AS fraction of the particle effloresces at a certain RH. With increasing 4-hydroxybenzoic acid mass fraction, no discontinuity step at the corresponding ERH in the dehydration curve of mixtures is observed. This suggests the presence of 4-hydroxybenzoic acid in the liquid state retards or offsets the efflorescence of AS in the mixtures. An interesting, yet contrasting phenomenon was observed for the hydration process of aerosol mixtures containing 4-hydroxybenzoic acid and AS by Lei et al. (2014). For the case of these mixtures during moistening, the deliquescence of ammonium sulfate in the mixed particles remains unaffected, within experimental resolution, by the presence of 4-hydroxybenzoic acid (Lei et al., 2014). Similar behavior has been observed for particles containing certain organic acids of limited water-solubility mixed ammonium sulfate (Choi and Chan, 2002; Chan and Chan, 2003). For example, mixtures for succinic acid + ammonium sulfate showed no substantial influence on the deliquescence RH of ammonium sulfate in the hydration process (Choi and Chan, 2002). However, a clear RH shift of the deliquescence phase transition of ammonium sulfate or sodium chloride was determined for mixed particles containing organic acids of higher water-solubility and O: C ratio, such as citric acid and malonic acid (e.g. Choi and Chan, 2002). The DRH and ERH of pure organics and AS in the mixed organic-AS particles are summarized in Table 4, the measurements indicate that 4-hydroxybenzoic acid has a significant effect on the efflorescence of AS when present in sufficient amount. Also, there is a clear reduction in the diameter growth factors prior to crystallization for mixtures with increasing 4-hydroxybenzoic acid mass fraction.

The measurements of mixtures consisting of 4-hydroxybenzoic acid and AS are compared with model predictions based on different assumptions about the phase state of the organic component, since the deviation from measurements might partly be explained by a transition in the physical state of the organic component. The E-AIM model prediction is referring to a system where the mixtures of 4-hydroxybenzoic acid is assumed to be in the liquid state at all RH levels, which the efflorescence of AS is considered. Neglecting the potential efflorescence of the organic component in the dehydration branch makes a systematic offset more obvious prior to the efflorescence of AS. A good E-AIM model-measurement agreement occurs below the predicted ERH of AS for mixed particles. The overestimation of HGFs before the efflorescence of AS is explained by the AIOMFAC model prediction with distinct assumptions about the organic phase state. A possible reason for the departure of model-measurement

agreement at $RH < 80\%$ is that there are two liquid-to-solid phase transitions, occurring in the mixed particles: a gradual one for the organic component and a step-like one for AS at lower RH. This phenomenon is shown in the grid square range in Fig. 4 and supported by comparison of the measured HGF data with AIOMFAC-based predictions for two assumptions about the organic phase state, especially in the case of mixtures with 50 and 75 wt-% organic. We acknowledge that the model predictions of the HGF curves for the two organic phase state assumptions differ within experimental error for the case shown in Fig. 4a, indicating that alternative explanations, such as model/measurement uncertainty in the absence of a liquid-solid phase transition could explain the observations. In the Fig. 4b, good agreement between measurements and the AIOMFAC model prediction with liquid organic assumption is found for $RH > 65\%$, while for $RH \leq 60\%$ the experimental data agree very well with the dashed red model curve for the case with consideration of a solid organic component. It suggests that crystallization followed by gradually increasing partitioning of organic from the solution to the solid organic phase occurs in the range from 70 % to 60 % RH under conditions of dehumidification. Similarly, a liquid-to-solid phase transition occurs for the organic: AS mass ratio of 3:1 cases in the range from 80 % to 50 % RH. Meanwhile, AS remains dissolved in a supersaturated aqueous solution phase. Moreover, the AIOMFAC-based equilibrium model predicts a liquid-liquid phase separation (LLPS) to occur at RH below $\sim 90\%$ for the calculation cases with the assumption of the organic in the liquid state (for all three organic mass fractions in Fig. 4). This prediction leads to a liquid phase enriched in 4-hydroxybenzoic acid with some water and AS dissolved and a coexisting liquid phase enriched in AS and water. The onset of the LLPS during dehumidification leads to the kink in the red model curve near 90 % RH, since the slope of the HGF curve with RH changes in a non-smooth manner at the point of the LLPS phase transition. This change in slope is not noticeable from the experimental data alone, but the model-measurement comparison for the range above 80 % RH shows very good agreement. The two liquid phases will likely remain separated until nucleation of a crystalline 4-hydroxybenzoic acid phase occurs followed by gradual partitioning of the organic acid to the solid phase with decreasing RH (to $\sim 50\%$ RH), at which point only a single liquid phase (an aqueous AS phase with a tiny amount of dissolved HA) will remain until efflorescence of AS occurs. Above $\sim 90\%$ RH, a single, homogeneous liquid phase is predicted to exist. Interestingly, this AIOMFAC model-measurement comparison (Fig. 4, especially panels b and c) provides reasonable evidence that 4-hydroxybenzoic acid remains dissolved and therefore in a liquid phase state at high RH in the mixed particles upon dehumidification (it is present in both liquid

phases below 90 % RH, but highly enriched in the AS-poor phase). In contrast, in the case of pure 4-hydroxybenzoic acid aerosol particles, particles exposed to initial RH of ≥ 90 % remain in the solid state (or crystallize at RH > 90 %) in the dehydration mode (Fig. 2c). What factors contribute to keeping the organic in the liquid solution? It is possible that the aerosols generated with those mixed solutions were allowing the 4-hydroxybenzoic acid to fully dissolve as the AS provides substantial particle phase water content (within short time) into which the organic can be dissolved and may then further contribute to water uptake associated with the organic's hygroscopicity (unlike in the case of the pure 4-hydroxybenzoic acid particles). The 4-hydroxybenzoic acid remains dissolved in the mixture, possibly supersaturated with respect to the crystalline organic state (similarly to how AS stays supersaturated at RH below the DRH during drying). We consider this a reasonable explanation for the observed HGF data from the HTDMA in comparison to the different AIOMFAC-based curves.

3.2.3 Mixed system: humic acid + ammonium sulfate

Figure 5 shows that the experimental diameter growth factors of mixtures consisting of humic acid (HA) and AS with dry mass ratios of 1:3, 1:1 or 3:1 decreases with increasing mass fraction of HA at RH > 35 %. For example, at 35 % RH the measured HGF are 1.1, 1.05, 1.05 for the particles consisting of 25 wt %, 50 wt % and 75 wt % humic acid. In comparison, the diameter growth factor of pure supersaturated AS particles is ~ 1.13 just prior to efflorescence of AS. Humic acid, unlike levoglucosan and 4-hydroxybenzoic acid aerosol particles, has no noticeable effect on the efflorescence point of AS in the mixed aerosol particles. Results of the ZSR model agrees well with measured hygroscopic growth for mixtures within the experimental error. The ZSR curves shown in Fig. 5 are based on the RH-dependent fitted hygroscopic growth factors of humic acid with Eq. (5) and the AIOMFAC predicted diameter growth factors of AS in the dehydration mode. The success of the ZSR mixing rule for this system suggests that interactions of organic molecules with ammonium sulfate ions in aqueous solution will only marginally affect the hygroscopic growth factors of the mixtures containing humic acid and AS. Due to the lack of detailed information about the actual chemical structures of humic acid samples used, it was not possible to perform E-AIM and AIOMFAC model predictions for comparison with the measurement.

3.3 Mixtures of biomass burning organic surrogate components with ammonium sulfate

According to Decesari et al, (2006), sampling of aerosol particles, including the WSOC fraction, was

conducted from September 9 to November 14, 2002 in their field study, the sampling time was subdivided into different periods. Despite of significant changes in the chemical composition of tracer compounds from the dry to the wet period, the functional groups and general chemical classes of WSOC changed only to a small extent in the Amazon basin near Rondônia, Brazil. Model compounds represent semi-quantitatively (presence/abundance of functional groups) and the chemical structure of WSOC can be used as surrogates in microphysical models involving organic aerosol particles over tropical areas affected by biomass burning scenarios (Andreae et al., 2002; Artaxo et al., 2002; Rissler et al., 2006; Decesari et al., 2006). Here, we focus on experimental observations and model calculations for relatively simple mixtures of inorganic-organic surrogate components reflecting mixtures of aerosol components found during different seasons during biomass burning events. However, we are fully aware of that fact that actual biomass burning aerosols are typically much more complex in terms of particle chemical composition. Aerosol particle properties from biomass burning events depend on the types of sources, external/internal population mixing state, water-solubilities, and phase state of the diversity of organic compounds and their mixing with inorganic constituents during different time periods in the field (e.g. Decesari et al., 2006).

3.3.1 Mixtures system: mix-bio-dry and mix-bio-wet aerosol particles

Figure 6a shows the observed small differences in the hygroscopicity parameter κ for mixtures of organic surrogate components and ammonium sulfate representing biomass burning particles during the dry and wet periods in the Amazon, respectively. Hygroscopicity parameter values for bio-mix-dry aerosol particles were determined to be between 0.16 and 0.18 with decreasing RH in the range from 90 % to 40 % RH. The κ value representing the wet period in the Amazon is shown in Fig. 6b, derived from laboratory HTDMA measurements in the range from 90 % to 40 % RH. A similar trend of an increase in κ with a decrease in RH has also been observed by Cheung et al. (2015). Their observation is based on ambient particle measurement with a HTDMA in Hong Kong, therefore probing particles of more complex compositions in the field campaign. The variability of the hygroscopicity parameter in sub-saturated conditions reveals some limitations of a single-parameter hygroscopicity model for applications over a wide range of RH. At low, intermediate and high RH levels, differing degrees of solution non-ideality, potential for liquid-liquid phase separation, water-solubility limitations of organics in ambient organic-inorganic particles, and assumptions about constant/variable surface tension may all play a role

(Mikhailov et al., 2009; Wex et al., 2009, Rastak et al., 2017; Ovadnevaite et al. 2017; Wang et al., 2017).

In the case of κ of organic surrogates mixed with ammonium sulfate, the relevant κ value range is ~ 0.12 to 0.15 obtained from 90% to 40% RH. The measured κ values of the mixtures are compared to field data of HTDMA and CCN measurements conducted at a remote rainforest site in the central Amazon during the dry and wet seasons (Whitehead et al., 2016; Pöhlker et al., 2016), which are consistent with κ obtained at similar field sites (within the uncertainty of experiments). The likely reason for a relatively good agreement between the hygroscopicity of the laboratory mixtures and the field data is that the organic mass fractions of the mix-bio-dry and mix-bio-wet mixtures are chosen in our laboratory experiments to be similar to those of the latest field data from Amazon. For example, Pöhlker et al. (2016) obtained the effective hygroscopicity parameters κ between 0.3 ± 0.01 and 0.15 ± 0.01 based on the organic mass fraction range from 0.65 to 0.97 in the dry season by aerosol chemical speciation monitor (ACSM) and CCN measurements. The predicted κ values of the mixtures at various RH levels shown in Fig. 6 (black curves) are obtained by application of Eq. (4) with use of the RH-dependent fitted HGFs of the organic surrogates (Eq. 5), the predicted growth factor of AS by the AIOMFAC model (for the humidification case) and the volume fraction based mixing rule for a mixture's HGF (Eq. 6). For these calculations, a solution surface tension of 0.072 J m^{-2} was assumed. These predictions agree relatively well with the experimental κ_{dry} and κ_{wet} values obtained from the HTDMA over a wide range in RH referring to dehumidification conditions (no solid AS). Furthermore, the combined approach of Eqs. (4-6) allows for a prediction of the change in κ at high RH towards water vapor super-saturation. A small difference in κ between sub- and super-saturated conditions is observed for our mixed systems when comparing the HTDMA data and predictions at 90% RH with the predictions near 100% RH and the κ values from the CNN field measurements. The difference is more pronounced for the wet season case. Rastak et al. (2017) observed a marked difference in apparent hygroscopicity and related mixture κ of the organic aerosols (AS-free) occurring in the case of monoterpene-derived secondary organic aerosol (SOA) for sub- vs. super-saturated conditions. A smaller difference was reported for the isoprene-derived SOA (Pajunoja et al., 2015; Rastak et al., 2017), more like the difference observed here for the mixtures containing AS (and therefore having overall higher κ values than typical salt-free organic aerosols). Rastak et al. (2017) attribute the distinct difference in κ_{SOA} of the monoterpene SOA to the limited mutual solubility of certain SOA components in water, because a single liquid organic-phase of monoterpene oxidation products is present at RH below 95% , but over a RH range above 95% , liquid-liquid phase

separation is observed by optical microscopy as well as predicted by the AIOMFAC-based equilibrium model. In the mix-bio-wet and mix-bio-dry cases shown in Fig. 6, the likely reason for the change in characteristic mixture hygroscopicity is not necessarily due to a liquid-liquid phase separation at high RH. For example, the κ parameter obtained from field data is $\sim 0.15 \pm 0.06$ at 90 % RH, while its value reaches $\sim 0.18 \pm 0.04$ at RH > 100 % (just prior to CCN activation). A likely reason for the difference is that hygroscopic particles, especially those containing sparingly soluble organics like 4-hydroxybenzoic acid, take up water dramatically above 95 % RH when approaching 100 % RH (Huff Hartz et al., 2006; Chan et al., 2008; Rastak et al., 2017), which is clear from model predictions, as demonstrated in Fig. 6 by application of Eq. (4). The predicted curve in the mixture's effective κ parameter may well capture the change in hygroscopicity under such high RH conditions. Consequently, for a precise representation of the hygroscopic growth behavior (e.g. HGF) at high RH (> 95 %) by the κ -Köhler model, the value of κ would need to be varied. While a variable κ value is contrary to the attempted simplicity of the single-parameter κ -Köhler model, it is at least advised to consider that κ values derived from HGF data at 80 % or 90 % RH may not apply accurately for the calculation of CCN activation properties of such biomass burning aerosols.

To summarize, there is small difference in hygroscopicity parameters between sub-saturated measurement conditions at 90 % RH in the laboratory with HTDMA and supersaturated conditions using CCN measurements, in agreement with the findings of other studies. At regional scale, in the dry and wet period, the hygroscopic behavior in some extent of the Amazon rainforest is influenced significantly by the biomass burning emissions, which enhances CCN activity and droplet number concentrations in warm clouds in that region and influences the radiation balance and cloud life time (Pöschl et al., 2010). Underestimation of organic surrogate component mass fractions in the mixed particles or organic:sulfate mass ratios may be responsible for the slight differences in the determined κ parameters of the laboratory and field measurements.

4. Conclusions

A number of field-based hygroscopicity studies about biomass burning aerosol focus on the growth factors of mixtures at high RH (e.g. 90 % RH). However, less attention has been paid to the growth

behavior at low to moderate RH, limiting the database for accurate estimates of particles optical and radiative properties over those lower RH ranges. However, this is a RH range in which water uptake or release behavior demonstrates a considerable variability among different organic-inorganic systems. The occurrence or suppression of a liquid-solid phase transition affects the physicochemical particle properties in a relative narrow RH range, potentially leading to particles of different morphology and physical states, affecting effective particle size and density. In this work, measurements and thermodynamic equilibrium predictions for organic-inorganic aerosols related to components from biomass burning emissions demonstrate a diversity of hygroscopic growth/shrinking behavior. For example, in the case of aerosol mixtures containing levoglucosan and ammonium sulfate, the presence of levoglucosan may cause the efflorescence of AS to occur at higher RH than in pure aqueous AS particles-or it may completely suppress AS efflorescence, as observed for mixtures with a high levoglucosan mass fraction. The growth curves predicted with an AIOMFAC-based thermodynamic equilibrium model reproduce the observations in most cases reasonably well and we demonstrate the usefulness of predictions with different assumptions about the physical state of the organic components for the interpretation of experimental data, such as in the case of mixtures of 4-hydroxybenzoic acid and ammonium sulfate. However, the accurate prediction of AS efflorescence or its suppression in mixed particles is difficult. The E-AIM-predicted growth curves reproduce the measured hygroscopic behavior relatively well for the consideration of the effect of 4-hydroxybenzoic acid on the hygroscopic behavior of mixtures with ammonium sulfate, which leads to suppression of the ammonium sulfate efflorescence. In the case of mixtures of humic acid and ammonium sulfate, continuous water desorption of aerosol particles shows no significant effect on the efflorescence of ammonium sulfate. Also, as expected, there is a clear reduction in the diameter growth factor of mixed systems, in comparison with that of pure AS particles. In addition, the small difference of hygroscopicity parameters of mix-bio-dry and mix-bio-wet systems between measured data in the laboratory using HTDMA and the field using CCN activity measurements is due to the similar O:C ratios of organic surrogate compounds and ammonium sulfate mass fractions used in the model mixtures when experimental κ data from sub- and super-saturated water vapor conditions are compared.

The range of measurement-model comparisons presented in this study indicate that providing accurate thermodynamic model predictions of the hygroscopic growth behavior of mixed organic-inorganic

systems remains a challenging problem. At moderate and low RH, where aerosol solution phases become highly concentrated, step-like or gradual crystallization and related solid-liquid equilibria may occur with high sensitivity to the organic/inorganic mass ratio and the chemical nature of the mixture constituents. To further improve thermodynamic equilibrium models for the prediction of hygroscopicity and phase transitions, controlled laboratory experiments with single solutes and/or with mixed organic-inorganic systems of known phase state will be useful to constrain model parameters. Ideally, such measurements should cover the high, intermediate and low RH ranges under humidification and dehumidification conditions.

Acknowledgements. This project was supported by the Strategic Priority Research Program (B) of the Chinese Academy of Sciences (Grant No. XDB05010400), the National Key Research and Development Program of China (2016YFC0202202), and the National Natural Science Foundation of China (Contract No. 91544227, 41227805). The authors would like to thank J. Hong and Z. B. Wang for comments and suggestions for improvement of the manuscript.

Reference

Altaf, M. B., Zuend, A., and Freedman, M. A.: Role of nucleation mechanism on the size dependent morphology of organic aerosol, *Chemical communications*, 52, 9220-9223, 2016.

Andreae, M. O. and Gelencser, A.: Black carbon or brown carbon? The nature of light-absorbing carbonaceous aerosols, *Atmospheric Chemistry and Physics*, 6, 3131-3148, 2006.

Apelblat, A.: The vapour pressures of saturated aqueous solutions of potassium bromide, ammonium sulfate, copper (II) sulfate, iron (II) sulfate, and manganese (II) dichloride, at temperatures from 283 K to 308 K, *The Journal of Chemical Thermodynamics*, 25, 1513-1520, 1993.

Arnold, S., Emmons, L., Monks, S., Law, K. S., Ridley, D., Turquety, S., Tilmes, S., Thomas, J. L., Bouarar, I., and Flemming, J.: Biomass burning influence on high-latitude tropospheric ozone and reactive nitrogen in summer 2008: a multi-model analysis based on POLMIP simulations, *Atmospheric*

683 Chemistry and Physics, 15, 6047-6068, 2015.

684 Artaxo, P., Martins, J. V., Yamasoe, M. A., Procópio, A. S., Pauliquevis, T. M., Andreae, M. O., Guyon,
685 P., Gatti, L. V., and Leal, A. M. C.: Physical and chemical properties of aerosols in the wet and dry
686 seasons in Rondônia, Amazonia, *Journal of Geophysical Research: Atmospheres*, 107, LBA 49-41-LBA
687 49-14, 2002.

688 Atkinson, D. B., Radney, J. G., Lum, J., Kolesar, K. R., Cziczo, D. J., Pekour, M. S., Zhang, Q., Setyan,
689 A., Zelenyuk, A., and Cappa, C. D.: Aerosol optical hygroscopicity measurements during the 2010
690 CARES campaign, *Atmospheric Chemistry and Physics*, 15, 4045-4061, 2015.

691 Bahadur, R., Praveen, P. S., Xu, Y. Y., and Ramanathan, V.: Solar absorption by elemental and brown
692 carbon determined from spectral observations, *Proceedings of the National Academy of Sciences of the*
693 *United States of America*, 109, 17366-17371, 2012.

694 Beyer, K. D., Friesen, K., Bothe, J. R., and Palet, B.: Phase Diagrams and Water Activities of Aqueous
695 Dicarboxylic Acid Systems of Atmospheric Importance, *Journal of Physical Chemistry A*, 112, 11704-
696 11713, 10.1021/jp805985t, 2008.

697 Bodsworth, A., Zobrist, B., and Bertram, A. K.: Inhibition of efflorescence in mixed organic-inorganic
698 particles at temperatures less than 250 K, *Physical chemistry chemical physics : PCCP*, 12, 12259-12266,
699 2010.

700 Bones, D. L., Reid, J. P., Lienhard, D. M., and Krieger, U. K.: Comparing the mechanism of water
701 condensation and evaporation in glassy aerosol, *Proceedings of the National Academy of Sciences*, 109,
702 11613-11618, 2012.

703 Boucher Olivier and David, R.: *Clouds and Aerosols*, PICC, 2013.

704 Brooks, S. D., DeMott, P. J., and Kreidenweis, S. M.: Water uptake by particles containing humic
705 materials and mixtures of humic materials with ammonium sulfate, *Atmos. Environ.*, 38, 1859-1868,
706 2004.

707 Carrico, C. M., Petters, M. D., Kreidenweis, S. M., Collett, J. L., Engling, G., and Malm, W. C.: Aerosol
708 hygroscopicity and cloud droplet activation of extracts of filters from biomass burning experiments,

709 Journal of Geophysical Research, doi:10.1029/2007JD009274, 2008.

710 Chan, M. N. and Chan, C. K.: Hygroscopic properties of two model humic-like substances and their
711 mixtures with inorganics of atmospheric importance, *Environmental Science & Technology*, 37, 5109-
712 5115, 2003.

713 Chan, M. N., Choi, M. Y., Ng, N. L., and Chan, C. K.: Hygroscopicity of water-soluble organic
714 compounds in atmospheric aerosols: Amino acids and biomass burning derived organic species,
715 *Environmental Science & Technology*, 39, 1555-1562, 2005.

716 Chan, M. N., Kreidenweis, S. M., and Chan, C. K.: Measurements of the Hygroscopic and Deliquescence
717 Properties of Organic Compounds of Different Solubilities in Water and Their Relationship with Cloud
718 Condensation Nuclei Activities, *Environmental Science & Technology*, 42, 3602-3608, 2008.

719 Chan, M. N. C. a. C. K.: Mass transfer effects in hygroscopic measurements of aerosol particles,
720 *Atmospheric Chemistry and Physics*, 2005. 2005.

721 Cheung, H. H. Y., Yeung, M. C., Li, Y. J., Lee, B. P., and Chan, C. K.: Relative Humidity-Dependent
722 HTDMA Measurements of Ambient Aerosols at the HKUST Supersite in Hong Kong, China, *Aerosol
723 Science and Technology*, 49, 643-654, 2015.

724 Cheng, Y. F., Su, H., Rose, D., Gunthe, S. S., Berghof, M., Wehner, B., Achtert, P., Nowak, A., Takegawa,
725 N., Kondo, Y., Shiraiwa, M., Gong, Y. G., Shao, M., Hu, M., Zhu, T., Zhang, Y. H., Carmichael, G. R.,
726 Wiedensohler, A., Andreae, M. O., and Pöschl, U.: Size-resolved measurement of the mixing state of soot
727 in the megacity Beijing, China: diurnal cycle, aging and parameterization, *Atmospheric Chemistry and
728 Physics*, 12, 4477-4491, 2012.

729 Choi, M. Y. and Chan, C. K.: The effects of organic species on the hygroscopic behaviors of inorganic
730 aerosols, *Environmental science & technology*, 36, 2422-2428, 2002.

731 Ciarelli, G., Aksoyoglu, S., Crippa, M., Jimenez, J. L., Nemitz, E., Sellegri, K., Äijälä, M., Carbone, S.,
732 Mohr, C., O'Dowd, C., Poulain, L., Baltensperger, U., and Prévôt, A. S. H.: Evaluation of European air
733 quality modelled by CAMx including the volatility basis set scheme, *Atmos. Chem. Phys.*, 16, 10313-
734 10332, 2016.

735 Ciobanu, V. G., Marcolli, C., Krieger, U. K., Zuend, A., and Peter, T.: Efflorescence of ammonium sulfate
736 and coated ammonium sulfate particles: evidence for surface nucleation, *The Journal of Physical*
737 *Chemistry A*, 114, 9486-9495, 2010.

738 Clegg, S. L. and Seinfeld, J. H.: Thermodynamic models of aqueous solutions containing inorganic
739 electrolytes and dicarboxylic acids at 298.15 K. 2. Systems including dissociation equilibria, *Journal of*
740 *Physical Chemistry A*, 110, 5718-5734, 2006.

741 Clegg, S. L. and Wexler, A. S.: Densities and Apparent Molar Volumes of Atmospherically Important
742 Electrolyte Solutions. 1. The Solutes H₂SO₄, HNO₃, HCl, Na₂SO₄, NaNO₃, NaCl, (NH₄)₂SO₄,
743 NH₄NO₃, and NH₄Cl from 0 to 50 degrees C, Including Extrapolations to Very Low Temperature and
744 to the Pure Liquid State, and NaHSO₄, NaOH, and NH₃ at 25 degrees C, *Journal of Physical Chemistry*
745 *A*, 115, 3393-3460, 2011a.

746 Clegg, S. L. and Wexler, A. S.: Densities and apparent molar volumes of atmospherically important
747 electrolyte solutions. 2. The systems H⁽⁺⁾-HSO₄⁽⁻⁾-SO₄⁽²⁻⁾-H₂O from 0 to 3 mol kg⁽⁻¹⁾ as a function of
748 temperature and H⁽⁺⁾-NH₄⁽⁺⁾-HSO₄⁽⁻⁾-SO₄⁽²⁻⁾-H₂O from 0 to 6 mol kg⁽⁻¹⁾ at 25 degrees C using a Pitzer ion
749 interaction model, and NH₄HSO₄·H₂O and (NH₄)₃H(SO₄)₂·H₂O over the entire concentration range, *The*
750 *journal of physical chemistry. A*, 115, 3461-3474, 2011b.

751 Decesari, S., Fuzzi, S., Facchini, M. C., Mircea, M., Emblico, L., Cavalli, F., Maenhaut, W., Chi, X.,
752 Schkolnik, G., Falkovich, A., Rudich, Y., Claeys, M., Pashynska, V., Vas, G., Kourtchev, I., Vermeylen,
753 R., Hoffer, A., Andreae, M. O., Tagliavini, E., Moretti, F., and Artaxo, P.: Characterization of the organic
754 composition of aerosols from Rondonia, Brazil, during the LBA-SMOCC 2002 experiment and its
755 representation through model compounds, *Atmospheric Chemistry and Physics*, 6, 375-402, 2006.

756 Denjean, C., Formenti, P., Picquet-Varrault, B., Pangui, E., Zapf, P., Katrib, Y., Giorio, C., Tapparo, A.,
757 Monod, A., and Temime-Roussel, B.: Relating hygroscopicity and optical properties to chemical
758 composition and structure of secondary organic aerosol particles generated from the ozonolysis of α-
759 pinene, *Atmospheric Chemistry and Physics*, 15, 3339-3358, 2015.

760 Dick, W. D., Saxena, P., and McMurry, P. H.: Estimation of water uptake by organic compounds in
761 submicron aerosols measured during the Southeastern Aerosol and Visibility Study, *Journal of*

762 Geophysical Research-Atmospheres, 105, 1471-1479, 2000.

763 Dusek, U., Frank, G. P., Massling, A., Zeromskiene, K., Iinuma, Y., Schmid, O., Helas, G., Hennig, T.,
764 Wiedensohler, A., and Andreae, M. O.: Water uptake by biomass burning aerosol at sub- and
765 supersaturated conditions: closure studies and implications for the role of organics, Atmospheric
766 Chemistry and Physics, 11, 9519-9532, 2011.

767 Engelhart, G. J., Hennigan, C. J., Miracolo, M. A., Robinson, A. L., and Pandis, S. N.: Cloud
768 condensation nuclei activity of fresh primary and aged biomass burning aerosol, Atmospheric Chemistry
769 and Physics, 12, 7285-7293, 2012.

770 Favez, O., Alfaro, S. C., Sciare, J., Cachier, H., and Abdelwahab, M. M.: Ambient measurements of light-
771 absorption by agricultural waste burning organic aerosols, Journal of Aerosol Science, 40, 613-620, 2009.

772 Feng, Y., Chen, Y., Guo, H., Zhi, G., Xiong, S., Li, J., Sheng, G., and Fu, J.: Characteristics of organic
773 and elemental carbon in PM_{2.5} samples in Shanghai, China, Atmospheric Research, 92, 434-442, 2009.

774 Frosch, M., Prisle, N. L., Bilde, M., Varga, Z., and Kiss, G.: Joint effect of organic acids and inorganic
775 salts on cloud droplet activation, Atmospheric Chemistry and Physics, 11, 3895-3911, 10.5194/acp-11-
776 3895-2011, 2011.

777 Gilman, J. B., Lerner, B. M., Kuster, W. C., Goldan, P. D., Warneke, C., Veres, P. R., Roberts, J. M., de
778 Gouw, J. A., Burling, I. R., and Yokelson, R. J.: Biomass burning emissions and potential air quality
779 impacts of volatile organic compounds and other trace gases from fuels common in the US, Atmos. Chem.
780 Phys., 15, 13915-13938, 2015.

781 Gupta, D., Eom, H. J., Cho, H. R., and Ro, C. U.: Hygroscopic behavior of NaCl–MgCl₂ mixture
782 particles as nascent sea-spray aerosol surrogates and observation of efflorescence during humidification,
783 Atmos. Chem. Phys., 15, 11273-11290, 2015.

784 Hanford, K. L., Mitchem, L., Reid, J. P., Clegg, S. L., Topping, D. O., and McFiggans, G. B.:
785 Comparative thermodynamic studies of aqueous glutaric acid, ammonium sulfate and sodium chloride
786 aerosol at high humidity, Journal of Physical Chemistry A, 112, 9413-9422, 10.1021/jp802520d, 2008.

787 Hecobian, A., Zhang, X., Zheng, M., Frank, N., Edgerton, E. S., and Weber, R. J.: Water-Soluble Organic

788 Aerosol material and the light-absorption characteristics of aqueous extracts measured over the
789 Southeastern United States, *Atmospheric Chemistry and Physics*, 10, 5965-5977, 2010.

790 Hegg, D. A., Warren, S. G., Grenfell, T. C., Doherty, S. J., and Clarke, A. D.: Sources of light-absorbing
791 aerosol in arctic snow and their seasonal variation, *Atmospheric Chemistry and Physics*, 10, 10923-10938,
792 2010.

793 Hodas, N., Zuend, A., Mui, W., Flagan, R., and Seinfeld, J.: Influence of particle-phase state on the
794 hygroscopic behavior of mixed organic-inorganic aerosols, *Atmospheric Chemistry and Physics*, 15,
795 5027-5045, 2015.

796 Hodas, N., Zuend, A., Schilling, K., Berkemeier, T., Shiraiwa, M., Flagan, R. C., and Seinfeld, J. H.:
797 Discontinuities in hygroscopic growth below and above water saturation for laboratory surrogates of
798 oligomers in organic atmospheric aerosols, *Atmos. Chem. Phys.*, doi: 10.5194/acp-16-12767-2016, 2016.

799 Jacobson, M. Z.: Effects of biomass burning on climate, accounting for heat and moisture fluxes, black
800 and brown carbon, and cloud absorption effects, *Journal of Geophysical Research-Atmospheres*, 119,
801 8980-9002, 2014.

802 Jedelský Jiri, L. i. H. e. y., Pavel Hynčica, and Ivan and Cibulka: Partial molar volumes of organic
803 solutes in water. IV. Benzoic and hydroxybenzoic acids at temperatures from T D 298 K to T D 498 K
804 and pressures up to 30 MPa, *J. Chem. Thermodynamics*, 32, 11, 2000.

805 Jing, B., Tong, S., Liu, Q., Li, K., Wang, W., Zhang, Y., and Ge, M.: Hygroscopic behavior of
806 multicomponent organic aerosols and their internal mixtures with ammonium sulfate, *Atmospheric*
807 *Chemistry and Physics*, 16, 4101-4118, 2016.

808 Kim, J., Ahlm, L., Yli-Juuti, T., Lawler, M., Keskinen, H., Tröstl, J., Schobesberger, S., Duplissy, J.,
809 Amorim, A., Bianchi, F., Donahue, N. M., Flagan, R. C., Hakala, J., Heinritzi, M., Jokinen, T., Kürten,
810 A., Laaksonen, A., Lehtipalo, K., Miettinen, P., Petäjä, T., Rissanen, M. P., Rondo, L., Sengupta, K.,
811 Simon, M., Tomé, A., Williamson, C., Wimmer, D., Winkler, P. M., Ehrhart, S., Ye, P., Kirkby, J., Curtius,
812 J., Baltensperger, U., Kulmala, M., Lehtinen, K. E. J., Smith, J. N., Riipinen, I., and Virtanen, A.:
813 Hygroscopicity of nanoparticles produced from homogeneous nucleation in the CLOUD experiments,
814 *Atmos. Chem. Phys.*, 16, 293-304, 2016.

815 Kiss, G., Tombácz, E., and Hansson, H.-C.: Surface Tension Effects of Humic-Like Substances in the
816 Aqueous Extract of Tropospheric Fine Aerosol, *Journal of Atmospheric Chemistry*, 50, 279-294, 2005.

817 Koop, T., Bookhold, J., Shiraiwa, M., and Poschl, U.: Glass transition and phase state of organic
818 compounds: dependency on molecular properties and implications for secondary organic aerosols in the
819 atmosphere, *Physical Chemistry Chemical Physics*, 13, 19238-19255, 2011.

820 Konovalov, I. B., Beekmann, M., Berezin, E. V., Petetin, H., Mielonen, T., Kuznetsova, I. N., and Andreae,
821 M. O.: The role of semi-volatile organic compounds in the mesoscale evolution of biomass burning
822 aerosol: a modeling case study of the 2010 mega-fire event in Russia, *Atmos. Chem. Phys.*, 15, 13269-
823 13297, 2015.

824 Laborde, M., Crippa, M., Tritscher, T., Juranyi, Z., Decarlo, P. F., Temime-Roussel, B., Marchand, N.,
825 Eckhardt, S., Stohl, A., Baltensperger, U., Prevot, A. S. H., Weingartner, E., and Gysel, M.: Black carbon
826 physical properties and mixing state in the European megacity Paris, *Atmospheric Chemistry and Physics*,
827 13, 5831-5856, 2013.

828 Lack, D. A., Bahreni, R., Langridge, J. M., Gilman, J. B., and Middlebrook, A. M.: Brown carbon
829 absorption linked to organic mass tracers in biomass burning particles, *Atmospheric Chemistry and*
830 *Physics*, 13, 2415-2422, 2013.

831 Lack, D. A., Bahreni, R., Langridge, J. M., Gilman, J. B., and Middlebrook, A. M.: Brown carbon
832 absorption linked to organic mass tracers in biomass burning particles, *Atmospheric Chemistry and*
833 *Physics*, 13, 2415-2422, 2013.

834 Lack, D. A., Langridge, J. M., Bahreini, R., Cappa, C. D., Middlebrook, A. M., and Schwarz, J. P.: Brown
835 carbon and internal mixing in biomass burning particles, *Proceedings of the National Academy of*
836 *Sciences of the United States of America*, 109, 14802-14807, 2012.

837 Lawson, S. J., Keywood, M. D., Galbally, I. E., Gras, J. L., Cainey, J. M., Cope, M. E., Krummel, P. B.,
838 Fraser, P. J., Steele, L. P., Bentley, S. T., Meyer, C. P., Ristovski, Z., and Goldstein, A. H.: Biomass
839 burning emissions of trace gases and particles in marine air at Cape Grim, Tasmania, *Atmos. Chem. Phys.*,
840 15, 13393-13411, 2015.

841 Lee, Y. N.: Airborne measurement of inorganic ionic components of fine aerosol particles using the
842 particle-into-liquid sampler coupled to ion chromatography technique during ACE-Asia and TRACE-P,
843 Journal of Geophysical Research, doi:10.1029/2002JD003265, 2003.

844 Lei, T., Zuend, A., Wang, W. G., Zhang, Y. H., and Ge, M. F.: Hygroscopicity of organic compounds from
845 biomass burning and their influence on the water uptake of mixed organic ammonium sulfate aerosols,
846 Atmospheric Chemistry and Physics, 14, 1-20, 2014.

847 Lienhard, D. M., Bones, D. L., Zuend, A., Krieger, U. K., Reid, J. P., and Peter, T.: Measurements of
848 thermodynamic and optical properties of selected aqueous organic and organic-inorganic mixtures of
849 atmospheric relevance, The journal of physical chemistry. A, 116, 9954-9968, 2012.

850 Liu, B. Y. H., Pui, D. Y. H., and Rubow, K. L. a. S., W.W.: ELECTROSTATIC EFFECTS IN AEROSOL
851 SAMPLING AND FILTRATION, Arm. occup. Hyg., 29, 251-269, 1985.

852 Liu, J. M., Scheuer, E., Dibb, J., Ziemba, L. D., Thornhill, K. L., Anderson, B. E., Wisthaler, A., Mikoviny,
853 T., Devi, J. J., Bergin, M., and Weber, R. J.: Brown carbon in the continental troposphere, Geophysical
854 Research Letters, 41, 2191-2195, 2014.

855 Liu, Q., Jing, B., Peng, C., Tong, S., Wang, W., and Ge, M.: Hygroscopicity of internally mixed multi-
856 component aerosol particles of atmospheric relevance, Atmos. Environ., 125, 69-77, 2016.

857 Malm, W. C. and Kreidenweis, S. M.: The effects of models of aerosol hygroscopicity on the
858 apportionment of extinction, Atmos. Environ., 31, 1965-1976, 1997.

859 MAN NIN CHAN, A. K. Y. L., AND and CHAN, C. K.: Responses of Ammonium Sulfate Particles
860 Coated with Glutaric Acid to Cyclic Changes in Relative Humidity: Hygroscopicity and Raman
861 Characterization, Environ.Sci.Technol., 40, 6893-6989, 2006.

862 Man Nin Chan, C. K. C.: Mass transfer effects on the hygroscopic growth of ammonium sulfate particles
863 with a water-insoluble coating, Atmos. Environ., doi: 10.1016/j.atmosenv.2007.01.047, 2007.

864 Marcolli, C. and Peter, T.: Water activity in polyol/water systems: new UNIFAC parameterization, Atmos.
865 Chem. Phys., 5, 1545-1555, 2005.

866 Marshall, F. H., Miles, R. E. H., Song, Y.-C., Ohm, P. B., Power, R. M., Reid, J. P., and Dutcher, C. S.:
867 Diffusion and reactivity in ultraviscous aerosol and the correlation with particle viscosity, *Chemical*
868 *Science*, 7, 1298-1308, 2016.

869 Martin, M., Tritscher, T., Juranyi, Z., Heringa, M. F., Sierau, B., Weingartner, E., Chirico, R., Gysel, M.,
870 Prevot, A. S. H., Baltensperger, U., and Lohmann, U.: Hygroscopic properties of fresh and aged wood
871 burning particles, *Journal of Aerosol Science*, 56, 15-29, 2013.

872 Mikhailov, E., Vlasenko, S., Rose, D., and Pöschl, U.: Mass-based hygroscopicity parameter interaction
873 model and measurement of atmospheric aerosol water uptake, *Atmospheric Chemistry and Physics*, 13,
874 717-740, 2013.

875 Mochida, M. and Kawamura, K.: Hygroscopic properties of levoglucosan and related organic compounds
876 characteristic to biomass burning aerosol particles, *Journal of Geophysical Research-Atmospheres*,
877 doi:10.1029/2004JD004962, 2004.

878 Moosmuller, H., Chakrabarty, R. K., and Arnott, W. P.: Aerosol light absorption and its measurement: A
879 review, *Journal of Quantitative Spectroscopy & Radiative Transfer*, 110, 844-878, 2009.

880 Paglione, M., Saarikoski, S., Carbone, S., Hillamo, R., Facchini, M. C., Finessi, E., Giulianelli, L.,
881 Carbone, C., Fuzzi, S., Moretti, F., Tagliavini, E., Swietlicki, E., Stenstrom, K. E., Prevot, A. S. H.,
882 Massoli, P., Canaragatna, M., Worsnop, D., and Decesari, S.: Primary and secondary biomass burning
883 aerosols determined by proton nuclear magnetic resonance (¹H-NMR) spectroscopy during the 2008
884 EUCAARI campaign in the Po Valley (Italy), *Atmospheric Chemistry and Physics*, 14, 5089-5110, 2014.

885 Pajunoja, A, AT Lambe, J Hakala, N Rastak, MJ Cummings, JF Brogan, L Hao, M Paramonov, J
886 Hong, NL Prisle, J Malila, S Romakkaniemi, KEJ Lehtinen, A Laaksonen, M Kulmala, P Massoli, TB
887 Onasch, NM Donahue, I Riipinen, P Davidovits, DR Worsnop, T Petäjä, and A
888 Virtanen (2015), Adsorptive uptake of water by semisolid secondary organic aerosols. *Geophys. Res.*
889 *Lett.*, 42, 3063–3068. doi: 10.1002/2015GL063142.

890 Ovadnevaite, J., Zuend, A., Laaksonen, A., Sanchez, K. J., Roberts, G., Ceburnis, D., Decesari, S.,
891 Rinaldi, M., Hodas, N., Facchini, M. C., Seinfeld, J. H., and O’ Dowd, C.: Surface tension prevails over
892 solute effect in organic-influenced cloud droplet activation, *Nature*, 546, 637-641, 10.1038/nature22806,

893 2017.

894 Peng, C., Chan, M. N., and Chan, C. K.: The hygroscopic properties of dicarboxylic and multifunctional
895 acids: Measurements and UNIFAC predictions, *Environmental Science & Technology*, 35, 4495-4501,
896 2001.

897 Petters, M. D. and. Kreidenweis, S. M.: A single parameter representation of hygroscopic growth and
898 cloud condensation nucleus activity, *Atmos. Chem. Phys.*, 7, 1961-1971, 2007.

899 Pöhlker, M. L., Pöhlker, C., Ditas, F., Klimach, T., Hrabe de Angelis, I., Araújo, A., Brito, J., Carbone,
900 S., Cheng, Y., and Chi, X.: Long-term observations of cloud condensation nuclei in the Amazon rain
901 forest–Part 1: Aerosol size distribution, hygroscopicity, and new model parametrizations for CCN
902 prediction, *Atmospheric Chemistry and Physics*, 16, 15709-15740, 2016.

903 Powelson, M. H., Espelien, B. M., Hawkins, L. N., Galloway, M. M., and De Haan, D. O.: Brown Carbon
904 Formation by Aqueous-Phase Carbonyl Compound Reactions with Amines and Ammonium Sulfate,
905 *Environmental Science & Technology*, 48, 985-993, 2014.

906 Pratt, K. A., Murphy, S. M., Subramanian, R., DeMott, P. J., Kok, G. L., Campos, T., Rogers, D. C.,
907 Prenni, A. J., Heymsfield, A. J., Seinfeld, J. H., and Prather, K. A.: Flight-based chemical characterization
908 of biomass burning aerosols within two prescribed burn smoke plumes, *Atmospheric Chemistry and*
909 *Physics*, 11, 12549-12565, 2011.

910 Pratt, K. A. and Prather, K. A.: Aircraft measurements of vertical profiles of aerosol mixing states, *Journal*
911 *of Geophysical Research*, doi:10.1029/2009JD013150, 2010.

912 Rastak, N., Pajunoja, A., Acosta Navarro, J. C., Ma, J., Song, M., Partridge, D. G., Kirkevåg, A., Leong,
913 Y., Hu, W. W., Taylor, N. F., Lambe, A., Cerully, K., Bougiatioti, A., Liu, P., Krejci, R., Petäjä, T., Percival,
914 C., Davidovits, P., Worsnop, D. R., Ekman, A. M. L., Nenes, A., Martin, S., Jimenez, J. L., Collins, D.
915 R., Topping, D. O., Bertram, A. K., Zuend, A., Virtanen, A., and Riipinen, I.: Microphysical explanation
916 of the RH-dependent water affinity of biogenic organic aerosol and its importance for climate,
917 *Geophysical Research Letters*, doi: 10.1002/2017GL073056. 2017.

918 Reid, J. P., Dennis-Smith, B. J., Kwamena, N.-O. A., Miles, R. E. H., Hanford, K. L., and Homer, C.

919 J.: The morphology of aerosol particles consisting of hydrophobic and hydrophilic phases: hydrocarbons,
 920 alcohols and fatty acids as the hydrophobic component, *Physical Chemistry Chemical Physics*, 13,
 921 15559-15572, 2011.

922 Renbaum-Wolff, L., Song, M., Marcolli, C., Zhang, Y., Liu, P. F., Grayson, J. W., Geiger, F. M., Martin,
 923 S. T., and Bertram, A. K.: Observations and implications of liquid–liquid phase separation at high relative
 924 humidities in secondary organic material produced by α -pinene ozonolysis without inorganic salts,
 925 *Atmos. Chem. Phys.*, 16, 7969-7979, 2016.

926 Rissler, J., Vestin, A., Swietlicki, E., Fisch, G., Zhou, J., Artaxo, P., and Andreae, M. O.: Size distribution
 927 and hygroscopic properties of aerosol particles from dry-season biomass burning in Amazonia,
 928 *Atmospheric Chemistry and Physics*, 6, 471-491, 2006.

929 Rizzo, L. V., Correia, A. L., Artaxo, P., Procopio, A. S., and Andreae, M. O.: Spectral dependence of
 930 aerosol light absorption over the Amazon Basin, *Atmospheric Chemistry and Physics*, 11, 8899-8912,
 931 2011.

932 Rose, D., Gunthe, S. S., Su, H., Garland, R. M., Yang, H., Berghof, M., Cheng, Y. F., Wehner, B., Achtert,
 933 P., Nowak, A., Wiedensohler, A., Takegawa, N., Kondo, Y., Hu, M., Zhang, Y., Andreae, M. O., and
 934 Poschl, U.: Cloud condensation nuclei in polluted air and biomass burning smoke near the mega-city
 935 Guangzhou, China -Part 2: Size-resolved aerosol chemical composition, diurnal cycles, and externally
 936 mixed weakly CCN-active soot particles, *Atmospheric Chemistry and Physics*, 11, 2817-2836, 2011.

937 Saarnio, K., Aurela, M., Timonen, H., Saarikoski, S., Teinila, K., Makela, T., Sofiev, M., Koskinen, J.,
 938 Aalto, P. P., Kulmala, M., Kukkonen, J., and Hillamo, R.: Chemical composition of fine particles in fresh
 939 smoke plumes from boreal wild-land fires in Europe, *Science of the Total Environment*, 408, 2527-2542,
 940 2010.

941 Sadezky, A., Muckenhuber, H., Grothe, H., Niessner, R., and Poschl, U.: Raman micro spectroscopy of
 942 soot and related carbonaceous materials: Spectral analysis and structural information, *Carbon*, 43, 1731-
 943 1742, 2005.

944 Saleh, R., Hennigan, C. J., McMeeking, G. R., Chuang, W. K., Robinson, E. S., Coe, H., Donahue, N.
 945 M., and Robinson, A. L.: Absorptivity of brown carbon in fresh and photo-chemically aged biomass-

946 burning emissions, *Atmospheric Chemistry and Physics*, 13, 7683-7693, 2013.

947 Saleh, R., Robinson, E. S., Tkacik, D. S., Ahern, A. T., Liu, S., Aiken, A. C., Sullivan, R. C., Presto, A.
 948 A., Dubey, M. K., Yokelson, R. J., Donahue, N. M., and Robinson, A. L.: Brownness of organics in
 949 aerosols from biomass burning linked to their black carbon content, *Nature Geoscience*, 7, 647-650, 2014.

950 Seinfeld, J. and Pandis, S.: *Atmospheric chemistry and physics*. Hoboken. NJ: Wiley, 2006.

951 Shantanu H. Jathar, A. M., Kekkey C. Barsabti, William E. Asher, James F. Pankow and Michael J.
 952 Kleeman: Water uptake by organic aerosol and its influence on gas/particle partitioning of secondary
 953 organic aerosol in the United States doi: 10.1016/j.atmosenv.2016.01.001, 2016.

954 Shiraiwa, M., Zuend, A., Bertram, A. K., and Seinfeld, J. H.: Gas-particle partitioning of atmospheric
 955 aerosols: interplay of physical state, non-ideal mixing and morphology, *Physical Chemistry Chemical*
 956 *Physics*, 15, 11441-11453, 2013.

957 Sjogren, S., Gysel, M., Weingartner, E., Baltensperger, U., Cubison, M. J., Coe, H., Zardini, A. A.,
 958 Marcolli, C., Krieger, U. K., and Peter, T.: Hygroscopic growth and water uptake kinetics of two-phase
 959 aerosol particles consisting of ammonium sulfate, adipic and humic acid mixtures, *Journal of Aerosol*
 960 *Science*, 38, 157-171, 2007.

961 Smith, M. L., Bertram, A. K., and Martin, S. T.: Deliquescence, efflorescence, and phase miscibility of
 962 mixed particles of ammonium sulfate and isoprene-derived secondary organic material, *Atmospheric*
 963 *Chemistry and Physics*, 12, 9613-9628, 2012.

964 Song, M., Marcolli, C., Krieger, U. K., Zuend, A., and Peter, T.: Liquid-liquid phase separation and
 965 morphology of internally mixed dicarboxylic acids/ammonium sulfate/water particles, *Atmospheric*
 966 *Chemistry and Physics*, 12, 2691-2712, 2012.

967 Song, M., Marcolli, C., Krieger, U. K., Zuend, A., and Peter, T.: Liquid-liquid phase separation in aerosol
 968 particles: Dependence on O:C, organic functionalities, and compositional complexity, *Geophysical*
 969 *Research Letters*, 39, doi:10.1029/2012GL052807, 2012.

970 Srinivas, B. and Sarin, M. M.: Brown carbon in atmospheric outflow from the Indo-Gangetic Plain: Mass
 971 absorption efficiency and temporal variability, *Atmos. Environ.*, 89, 835-843, 2014.

972 Srinivas, B. and Sarin, M. M.: Light absorbing organic aerosols (brown carbon) over the tropical Indian
 973 Ocean: impact of biomass burning emissions, *Environmental Research Letters*, doi:10.1088/1748-
 974 9326/8/4/044042, 2013.

975 Svenningsson, B., Rissler, J., Swietlicki, E., Mircea, M., Bilde, M., Facchini, M. C., Decesari, S., Fuzzi,
 976 S., Zhou, J., Monster, J., and Rosenorn, T.: Hygroscopic growth and critical supersaturations for mixed
 977 aerosol particles of inorganic and organic compounds of atmospheric relevance, *Atmospheric Chemistry*
 978 *and Physics*, 6, 1937-1952, 2006.

979 Topping, D., McFiggans, G., and Coe, H.: A curved multi-component aerosol hygroscopicity model
 980 framework: Part 1–Inorganic compounds, *Atmospheric Chemistry and Physics*, 5, 1205-1222, 2005.

981 Tuckermann, R. a. C., H. K.: The surface tension of aqueous solutions of some atmospheric water-soluble
 982 organic compounds, *Atmos. Environ.*, 38, 6135-6138, 2004.

983 Väkevä, M., Kulmala, M., Stratmann, F., and Hämeri, K.: Field measurements of hygroscopic properties
 984 and state of mixing of nucleation mode particles, *Atmospheric Chemistry and Physics*, 2, 55-66, 2002.

985 Veghte, D. P., Altaf, M. B., and Freedman, M. A.: Size dependence of the structure of organic aerosol,
 986 *Journal of the American Chemical Society*, 135, 16046-16049, 2013.

987 Gonçalves, W. A., Machado, L. A. T., and Kirstetter, P.-E.: Influence of biomass aerosol on precipitation
 988 over the Central Amazon: an observational study, *Atmos. Chem. Phys.*, doi: 10.5194/acp-15-6789-2015,
 989 2015.

990 Wang, J., Cubison, M. J., Aiken, A. C., Jimenez, J. L., and Collins, D. R.: The importance of aerosol
 991 mixing state and size-resolved composition on CCN concentration and the variation of the importance
 992 with atmospheric aging of aerosols, *Atmospheric Chemistry and Physics*, 10, 7267-7283, 2010.

993 Wang, X., Heald, C. L., Ridley, D. A., Schwarz, J. P., Spackman, J. R., Perring, A. E., Coe, H., Liu, D.,
 994 and Clarke, A. D.: Exploiting simultaneous observational constraints on mass and absorption to estimate
 995 the global direct radiative forcing of black carbon and brown carbon, *Atmospheric Chemistry and Physics*,
 996 14, 10989-11010, 2014.

997 Whitehead, J. D., Darbyshire, E., Brito, J., Barbosa, H. M., Crawford, I., Stern, R., Gallagher, M. W.,

998 Kaye, P. H., Allan, J. D., and Coe, H.: Biogenic cloud nuclei in the central Amazon during the transition
999 from wet to dry season, *Atmospheric Chemistry and Physics*, 16, 9727-9743, 2016.

1000 Wu, Z. J., Zheng, J., Shang, D. J., Du, Z. F., Wu, Y. S., Zeng, L. M., Wiedensohler, A., and Hu, M.:
1001 Particle hygroscopicity and its link to chemical composition in the urban atmosphere of Beijing, China,
1002 during summertime, *Atmos. Chem. Phys.*, 16, 1123-1138, 2016.

1003 Yates III, L. M., Wandruszka, R.V.: Decontamination of polluted water by treatment with a crude humic
1004 acid blend, *Environmental Science and Technology*, 33, 2076-2080, 1999.

1005 You, Y. and Bertram, A. K.: Effects of molecular weight and temperature on liquid–liquid phase
1006 separation in particles containing organic species and inorganic salts, *Atmospheric Chemistry and*
1007 *Physics*, 15, 1351-1365, 2015.

1008 You, Y., Renbaum-Wolff, L., and Bertram, A. K.: Liquid–liquid phase separation in particles containing
1009 organics mixed with ammonium sulfate, ammonium bisulfate, ammonium nitrate or sodium chloride,
1010 *Atmospheric Chemistry and Physics*, 13, 11723-11734, 2013.

1011 Yuan Youa, L. R.-W., Marc Carreras-Sospedrab, Sarah J. Hannaa, Naruki Hiranumac, Saeid Kamald.,
1012 Mackenzie L. Smithe, X. Z., Rodney J. Weberf, John E. Shillingg, Donald Dabdubb, Scot T. Martine,h,1.,
1013 and Bertrama, a. A. K.: Images reveal that atmospheric particles can undergo liquid–liquid phase
1014 separations, *pnas*, 109, 13188-13193, 2012.

1015 Zamora, I. R., Tabazadeh, A., Golden, D. M., and Jacobson, M. Z.: Hygroscopic growth of common
1016 organic aerosol solutes, including humic substances, as derived from water activity measurements,
1017 *Journal of Geophysical Research: Atmospheres*, doi:10.1029/2011JD016067, 2011.

1018 Zardini, A. A., Sjogren, S., Marcolli, C., Krieger, U. K., Gysel, M., Weingartner, E., Baltensperger, U.,
1019 and Peter, T.: A combined particle trap/HTDMA hygroscopicity study of mixed inorganic/organic aerosol
1020 particles, *Atmospheric Chemistry and Physics*, 8, 5589-5601, 2008.

1021 Zawadowicz, M., Proud, S., Seppalainen, S., and Cziczo, D.: Hygroscopic and phase separation
1022 properties of ammonium sulfate/organics/water ternary solutions, *Atmospheric Chemistry and Physics*,
1023 15, 8975-8986, 2015.

1024 Zhang, Q., Jimenez, J. L., Canagaratna, M. R., Allan, J. D., Coe, H., Ulbrich, I., Alfarra, M. R., Takami,
1025 A., Middlebrook, A. M., Sun, Y. L., Dzepina, K., Dunlea, E., Docherty, K., DeCarlo, P. F., Salcedo, D.,
1026 Onasch, T., Jayne, J. T., Miyoshi, T., Shimo, A., Hatakeyama, S., Takegawa, N., Kondo, Y., Schneider,
1027 J., Drewnick, F., Borrmann, S., Weimer, S., Demerjian, K., Williams, P., Bower, K., Bahreini, R., Cottrell,
1028 L., Griffin, R. J., Rautiainen, J., Sun, J. Y., Zhang, Y. M., and Worsnop, D. R.: Ubiquity and dominance
1029 of oxygenated species in organic aerosols in anthropogenically-influenced Northern Hemisphere
1030 midlatitudes, *Geophysical Research Letters*, doi:10.1029/2007GL029979, 2007.

1031 Zhang, S. L., Ma, N., Kecorius, S., Wang, P. C., Hu, M., Wang, Z. B., Groß, J., Wu, Z. J., and
1032 Wiedensohler, A.: Mixing state of atmospheric particles over the North China Plain, *Atmos. Environ.*,
1033 125, Part A, 152-164, 2016.

1034 Zhong, M. and Jang, M.: Dynamic light absorption of biomass-burning organic carbon photochemically
1035 aged under natural sunlight, *Atmospheric Chemistry and Physics*, 14, 1517-1525, 2014.

1036 Zuend, A., Marcolli, C., Booth, A. M., Lienhard, D. M., Soonsin, V., Krieger, U. K., Topping, D. O.,
1037 McFiggans, G., Peter, T., and Seinfeld, J. H.: New and extended parameterization of the thermodynamic
1038 model AIOMFAC: calculation of activity coefficients for organic-inorganic mixtures containing carboxyl,
1039 hydroxyl, carbonyl, ether, ester, alkenyl, alkyl, and aromatic functional groups, *Atmospheric Chemistry
1040 and Physics*, 11, 9155-9206, 2011.

1041 Zuend, A., Marcolli, C., Luo, B. P., and Peter, T.: A thermodynamic model of mixed organic-inorganic
1042 aerosols to predict activity coefficients, *Atmospheric Chemistry and Physics*, 8, 4559-4593, 2008.

1043 Zuend, A., Marcolli, C., Peter, T., and Seinfeld, J. H.: Computation of liquid-liquid equilibria and phase
1044 stabilities: implications for RH-dependent gas/particle partitioning of organic-inorganic aerosols,
1045 *Atmospheric Chemistry and Physics*, 10, 7795-7820, 2010.

1046 Zuend, A. and Seinfeld, J. H.: Modeling the gas-particle partitioning of secondary organic aerosol: the
1047 importance of liquid-liquid phase separation, *Atmospheric Chemistry and Physics*, 12, 3857-3882, 2012.

1048

1049

1050

Chemical compound	Chemical formula	Molar Mass [g mol ⁻¹]	Density in solid or liquid state [g cm ⁻³]	Solubility g/100cm ³ H ₂ O	Solution surface tension [J m ⁻²]	Manufacturer
Ammonium sulfate	(NH ₄) ₂ SO ₄	132.140	1.770 ^a (solid), 1.550 ^a (liquid)	74.400(at 20°C)	0.072(0.001- 10mg/mL)	Alfa Aesar, 99.95%
Levoglucosan	C ₆ H ₁₀ O ₅	126.100	1.618 ^b (solid) 1.512 ^b (liquid)		0.073 ^c (0.01- 10mg/mL)	Aldrich, 99%
4-Hydroxybenzoic acid	C ₇ H ₆ O ₃	138.100	1.460(solid) 1.372 ^f (liquid)	0.675(at 25°C)	0.070 ^g (>10mg/mL)	Alfa Aesar, 99.99%
Humic acid		NA	0.800 ^h (solid)	NA	NA	Aldrich, 99%

1052 ^aClegg and Wexler, (2011);
1053 ^bLienhard et al, (2012);
1054 ^cTuckermann and Cammenga (2004) at 293K;
1055 ^fJedelsky et al, (2000);
1056 ^gKiss et al, (2005);
1057 ^hYates III and Wandruszka, (1999);
1058
1059
1060
1061
1062
1063
1064
1065
1066
1067
1068

1069 **Table 2.** The chemical composition of biomass-burning model mixtures studied given as mass
1070 percentages (wt %).

Mixture name	Levoglucosan	4-Hydroxybenzoic acid	Humic acid	Ammonium sulfate
Mix-bio-dry	87.2%	9.2%	1.5%	2.1%
Mix-bio-wet	68.0%	26.0%	3.0%	3.0%

1071
1072
1073
1074
1075
1076
1077
1078
1079
1080
1081
1082
1083
1084
1085
1086
1087

1088

1089

1090

1091

1092

1093

1094

1095

1096

1097

1098

1099

1100

1101

1102

1103

1104

1105

1106

Table 3. Coefficients (c_1 , c_2 , c_3) of the fitted growth factor parameterization (Eq. 5) as follows:

Chemical compounds	c_1	c_2	c_3
Levoglucosan	0.12868746	0.36582023	-0.39840382
4-Hydroxybenzoic acid	-1.389967E-01	2.325586E-01	-9.891943E-02
Humic acid	-1.618304E-02	2.202483E-01	2.005134E-02

1107 **Table 4:** Experimental studies of organic and ammonium sulfate (AS) deliquescence and efflorescence
1108 RH from this work and previous studies at 298K.

Signal compound/Mixture	Organic mass fraction (%)	Deliquescence relative humidity of AS or organic in the mixed particle	Efflorescence relative humidity of AS or organic in the mixed particle
Levogluconan	-	80% ^{a*} 82.8% ^b	< 4% ^{a*}
Levogluconan+AS	25	80%	45%
	50	-	-
	75	-	-
4-hydroxybenzoic acid	-	> 97% ^{a*}	< 4% ^{a*}
4-Hydroxybenzoic acid+AS	25	80%	35%
	50	80%	25%
	75	80%	-
Humic acid	-	-	-
Humic acid+AS	20	80%	35%
	50	80%	35%
	75	80%	35%

1109 ^{*}is the DRH and ERH of pure organic components.

1110 ^aMochida and Kawamura. (2004)

1111 ^bZamora et al. (2011)

1112

1113

1114

1115

1116

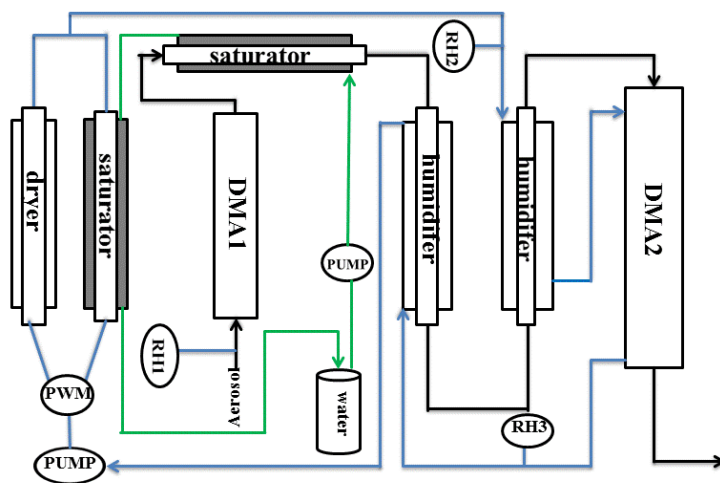


Figure 1. Schematic of the hygroscopicity tandem differential mobility analyzer (HTDMA) system. the sheath flow, aerosol flow, and water flow have been represented by the blue, black, green line, respectively. PWM: Pulse Width Modulator circuit.

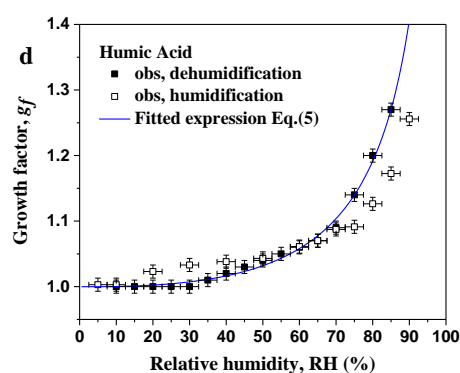
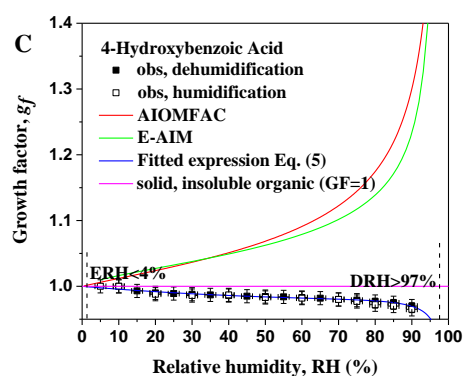
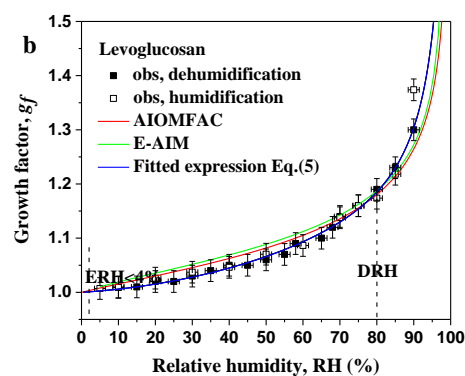
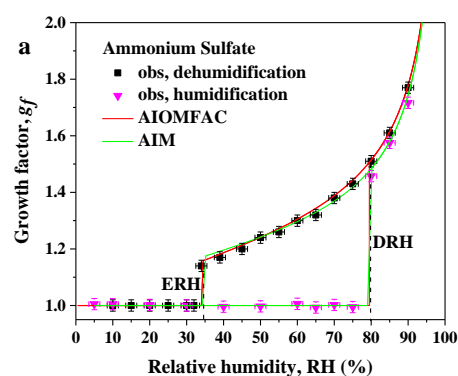


Figure 2. Hygroscopic growth, deliquescence and efflorescence of aerosol particles. Hygroscopic growth factors of (a) ammonium sulfate (AS), (b) levoglucosan, (c) 4-hydroxybenzoic acid, and (d) humic acid aerosol particles with dry diameter of 100 nm (open, black square). In this study, the green curves show E-AIM predictions, and the red curves the AIOMFAC predictions, and the blue lines the fitted expression (Eq. 5).

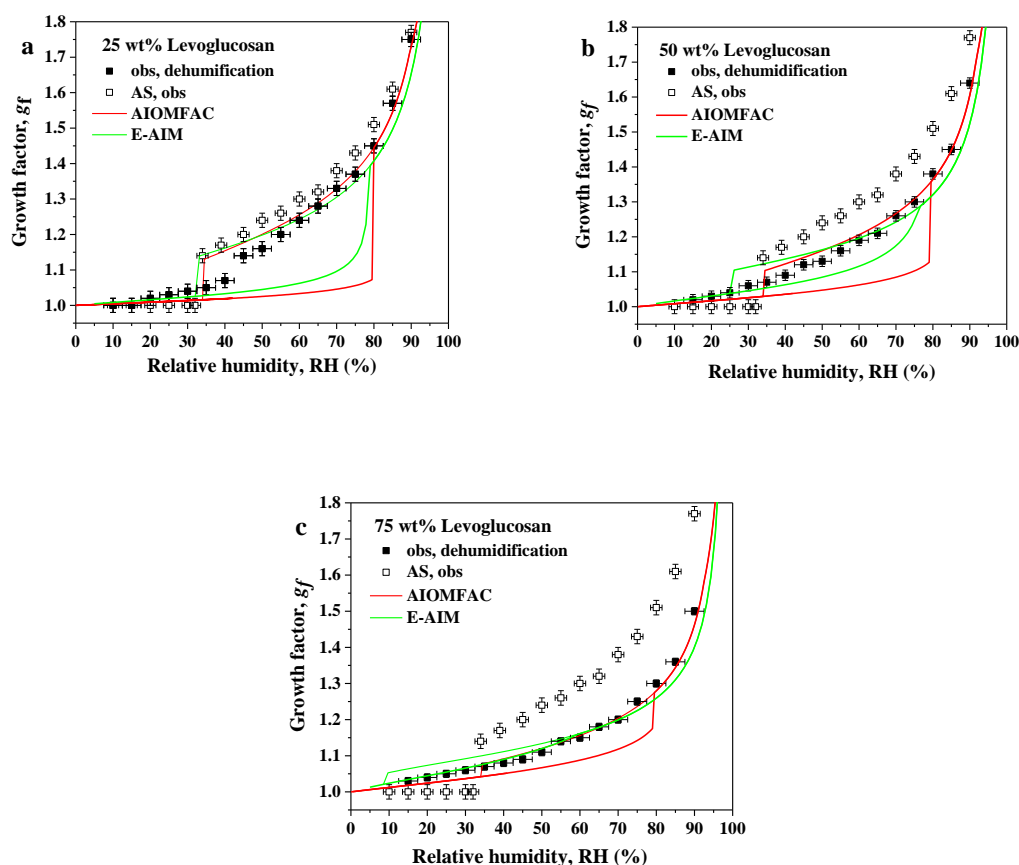


Figure 3. Hygroscopic growth, efflorescence of aerosol particles, and model predictions represent the diameter growth factor during dehydration experiments in the range from 90 % to 5 % RH at 298.15 K. (a,b,c). Hygroscopic growth curves of mixtures consisting of levoglucosan and ammonium sulfate (solid symbols) at three different dry state mass fraction for particles of an initial dry diameter of 100 nm at RH < 5 % as compared to that of pure ammonium sulfate (open symbols, “AS, obs”). AIOMFAC-based model predictions for bulk systems are shown in red, E-AIM predictions are shown in green.

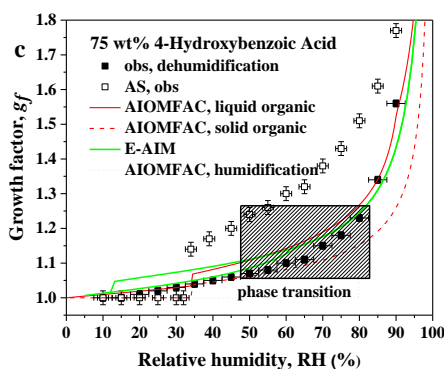
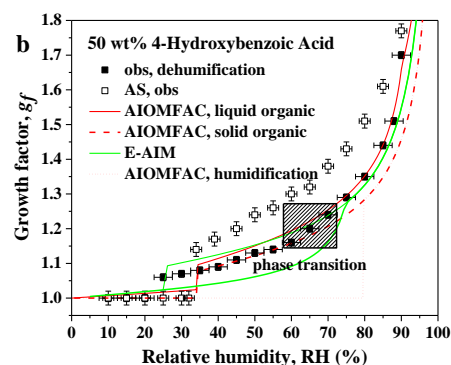
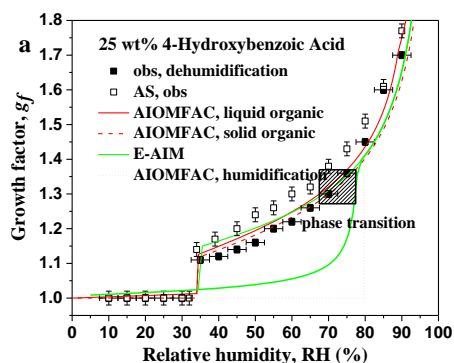


Figure 4. Hygroscopic growth factors, efflorescence of behavior, and model predications for dehydration experiments in the range from 90 % to 5 % RH at 298.15 K. (a,b,c) hygroscopic growth curves of mixtures consisting of 4-hydroxybenzoic acid and ammonium sulfate (solid symbols) at three different dry state mass fraction (initial dry diameter of 100 nm at RH < 5 %) as compared to that of pure ammonium sulfate (open symbols). AIOMFAC-based model predictions for bulk systems are shown in red, E-AIM-predictions are shown in green for the case of assuming that 4-hydroxybenzoic acid remains in the liquid state. Shaded rectangle: RH range of gradual crystallization of 4-hydroxybenzoic acid.

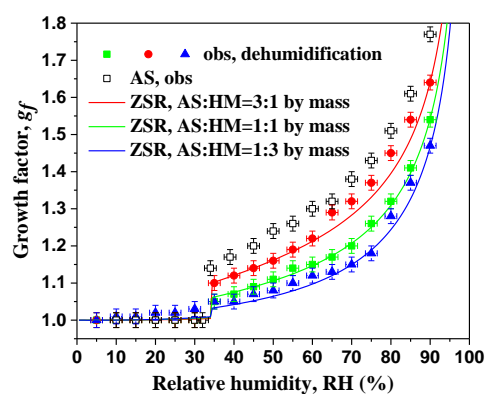


Figure 5. Hygroscopic growth factors, efflorescence of aerosol particles/constituents consisting of humic acid and ammonium sulfate at three different dry state mass fractions with initial dry diameter of 100 nm at $RH < 5\%$ as compared to that of pure ammonium sulfate (open symbols). Colored curves: ZSR predictions of diameter growth factors for dry particle compositions corresponding to the experimental data during dehumidification in the range from 90 % to 5 % RH at 298.15 K.

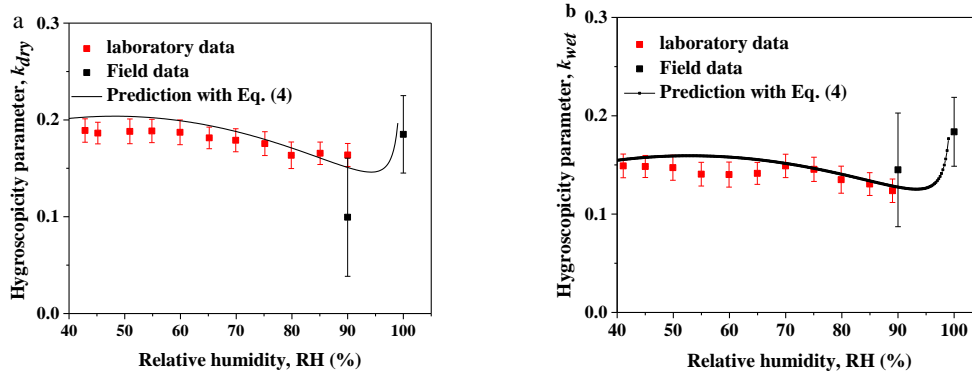


Figure 6. Hygroscopicity parameter, κ , representing mixed aerosol particles consisting of organic surrogate components and ammonium sulfate at different periods (initial dry diameter of 100 nm at RH < 5 %). The black curves in panels (a, b) show the κ prediction from Eq. (4) with HGF_{mix} calculated by Eq. (6) using component volume fractions and the HGF of the individual mixture components from a fit to the laboratory data (using Eq.5). the black symbols and error bars show field data from the Amazon during the dry and wet periods at conditions of water vapor sub-saturation (HTDMA measurement) and super-saturation (κ_{CNN}) (Whitehead et al., 2016; Pöhlker et al., 2006).